Title: Hyperactive PLCG1 drives non-canonical signaling to promote cell survival

Author: Longhui Zeng[1], Xinyan Zhang[1], Yiwei Xiong[1], Kazuki Sato[1], Nicole Hajicek[2], John Sondek[2], and Xiaolei Su[1,3,4,5,6]

1. Department of Cell Biology, Yale School of Medicine, New Haven, CT, USA

2. Department of Pharmacology, The University of North Carolina at Chapel Hill, Chapel Hill, NC, USA

3. Yale Cancer Center, New Haven, CT, USA

4. Yale Center for Immuno-Oncology, New Haven, CT, USA

5. Yale Center for Systems and Engineering Immunology, New Haven, CT, USA

6. Yale Stem Cell Center, New Haven, CT, USA

Correspondence: Xiaolei Su

Xiaolei.su@yale.edu

Abstract

One of the long-standing questions in cell signaling field to identify and characterize key signaling nodes out of a complex network. Phospholipase Cγ1 (*PLCG1*) was identified as the most frequently mutated gene in adult T-cell leukemia/lymphoma, suggesting a critical function of PLCG1 in driving T cell activation. However, it remains unclear how these mutations regulate T cell physiology and pathology. Here we investigated three common leukemia/lymphoma associated mutations (R48W, S345F, and D1165H). We discovered that these mutations induced hyperactive T cell signaling and caused pro-survival phenotypes. PLCG1 mutants enhanced LAT condensation, calcium influx, and ERK activation. They promoted T cell proliferation, induced cell aggregation, and rendered resistance to vorinostat, an FDA-approved drug for cutaneous T-cell lymphoma. The resistance to vorinostat depended on ERK signaling and can be reversed with an ERK inhibitor. Mechanistically, alpha smooth muscle actin, which was specifically induced by PLCG1 mutants, directly bound PLCG1 to promote its activation. Together, these results demonstrated that hyperactive PLCG1 promoted T cell survival and drug resistance through inducing non-canonical signaling.

Keywords

Actin/Condensation/ERK/PLCG1/T cell

Introduction

Phospholipase Cγ1 (PLCG1) protein serves as a key signaling molecule linking the upstream activation of transmembrane receptors (e.g. TCR, EGFR, PDGFR) to the downstream pathways leading to cytoskeleton remodeling, membrane fusion, and transcriptional induction(Chen & Simons, 2021). In T lymphocytes, TCR activation leads to the phosphorylation of LAT, a transmembrane adaptor protein(Zhang et al, 1998) that forms biomolecular condensation to promote TCR signaling(Huang et al, 2019; Su et al, 2016). Phosphorylated LAT recruits PLCG1 to the plasma membrane, resulting in the hydrolysis of PIP_2 to generate IP_3 and DAG, which induce calcium influx and MAPK signaling(Balagopalan et al, 2015; Courtney et al, 2018).

PLCG1 is a multi-domain phospholipase that has both enzyme-dependent and independent functions. The high-resolution structure of essentially full-length PLCG1(Hajicek et al, 2019) revealed the three-dimensional arrangement of PLCG1 domains. The regulatory domain cluster, which is composed of the sPH, nSH2, cSH2, and SH3 domains, interacts with the catalytic core to mask the substrate-binding site. When Y783 is phosphorylated (potentially by Itk(Qi & August, 2007)), it binds the cSH2 domain, triggering a conformational change that leads to the exposure of the catalytic site so that PLCG1 cleaves PIP_2 to generate the second messengers IP_3 and DAG(Gresset et al, 2010; Hajicek et al, 2019). In addition to the enzyme-dependent function, PLCG1 also has a scaffolding function: the nSH2, cSH2, and SH3 domains interact with LAT and Sos1 to promote condensation of the LAT complex and enhance TCR signal transduction(Wada et al, 2022; Zeng et al, 2021).

The pathological relevance of PLCG1 signaling was revealed by genome profiling of clinical samples. PLCG1 mutations were identified in cutaneous T-cell lymphoma(Patel et al, 2020; Vaque et al, 2014), angioimmunoblastic T-cell lymphoma(Wang et al, 2017), angiosarcoma(Behjati et al, 2014), and immune dysregulation diseases(Tao et al, 2023). Notably, PLCG1 is the most frequently mutated gene in adult T-cell leukemia/lymphoma (ATLL); about 36% of patients acquired mutations in PLCG1(Kataoka et al, 2015). This suggested PLCG1 as a key signaling molecule involved in T cell malignancy. The point mutations identified in ATLL spread along the entire PLCG1 with a few high-frequency spots. Namely, R48W sits on an N-terminal PH domain that potentially interacts with plasma membranes(Falasca et al, 1998). S345F is in the catalytic TIM barrel whereas D1165H is located on the C-terminal C2 domain that interacts with the membrane through calcium (**Fig. 1A**)(Ananthanarayanan et al, 2002; Lomasney et al, 2012). Although it remains unclear how R48W affects the conformation of PLCG1, both S345F and D1165H are located at the interface between the regulatory cluster and catalytic core; these mutations are expected to favor an open conformation of PLCG1(Hajicek et al, 2019). Indeed, biochemical assays showed an enhanced lipase activity of all three mutants(Hajicek et al, 2019). Moreover, these mutants trigger enhanced signaling downstream of PLCG1 including NFAT, AP-1, and NF-kB in cell line models(Patel et al, 2020; Vaque et al, 2014). However, it remains unclear whether hyperactivation of PLCG1 is sufficient to drive T cell proliferation and reduce cell death. The mechanisms by which these mutants contribute to cellular phenotypes linked to tumor progression also remain largely unexplored. Additionally, it remains unknown whether the signaling

and phenotypes induced by hyperactive PLCG1 simply mimic those triggered by TCR activation, or if novel functions of PLCG1 may arise outside of the TCR signaling network.

Therefore, we decided to investigate the mechanism and cellular consequence of hyperactive PLCG1 signaling using these ATLL-related mutants. We found that PLCG1 mutations enhanced LAT condensation, calcium influx and ERK phosphorylation. They promoted the activation and proliferation of human primary T cells. Using the T cell lymphoma line Hut78 as a model, we found that PLCG1 mutants induced cell aggregation by enhancing ICAM-1 expression. ICAM-1 engaged with integrin LAF-1 to increase ERK activation. The hyperactive ERK rendered cell resistance to vorinostat, an FDA-approved drug for cutaneous T-cell lymphoma and this resistance to vorinostat can be reversed by an ERK inhibitor. To determine if hyperactive PLCG1 induces signaling beyond canonical TCR network, we performed gene expression profiling and found genes in smooth muscle contraction were specifically induced by PLCG1 mutants but not TCR-stimulated wild-type samples. Alpha smooth muscle actin, which is highly expressed in PLCG1 mutants, directly bound PLCG1 and promoted the activation of PLCG1. Together, our work revealed how hyperactive PLCG1 affects T cell signaling and drug resistance to uncover insights on the pathogenesis mechanism of T-cell leukemia and lymphoma. Our work also highlights the neo-signaling induced by hyperactive PLCG1 mutants beyond traditional TCR signaling network.

Results

PLCG1 acquiring ATLL-associated mutations promoted LAT condensation *in vitro*

Our previous work demonstrated that PLCG1 promotes LAT condensation and enhances signaling beyond its lipase function in generating second messengers IP_3 and DAG. This is achieved through crosslinking LAT and binding partner Sos1 via the SH2 and SH3 domains on PLCG1(Zeng et al, 2021). To determine how ATLL mutations of PLCG1 affect LAT condensation, we implemented a supported lipid bilayer-based reconstitution assay that we developed before(Su et al, 2017; Zeng & Su, 2023). Briefly, the cytoplasmic domain of LAT was purified and phosphorylated by ZAP70 at four key tyrosine sites(Su et al, 2017), labeled with maleimide-Cy3B on a C-terminal cysteine, and attached to a Ni-NTA functionalized supported lipid bilayer through an N-terminal polyhistidine tag. The wild-type and three mutants of PLCG1 (R48W, S345F, and D1165H), together with Grb2 and Sos1 were purified as described before(Hajicek et al, 2019; Zeng et al, 2021) (**Fig. S1A**) and added in solution. Total internal reflection fluorescence (TIRF) microscopy was implemented to monitor LAT condensation with PLCG1, Grb2, and Sos1 (**Fig. 1B**) under physiologically relevant concentrations(Zeng et al, 2021). Interestingly, all three PLCG1 mutants induced higher condensation of LAT as compared to the wild-type PLCG1 (**Fig. 1C, 1D**). This can be potentially explained by the open conformation of PLCG1 mutants which renders more accessibility of their SH2 domain to the phosphotyrosines on LAT(Hajicek et al, 2019). To determine how PLCG1 mutants affect material property of LAT condensates, we performed fluorescence recovery after photobleaching (FRAP) analysis on LAT condensates. No significant difference was found between the wild-type and mutants (**Fig. S1B**), suggesting the

liquid-like property of LAT condensates remained similar between the wild-type and mutants. Together, data from biochemical reconstitution suggested that PLCG1 mutants directly enhanced LAT condensation.

PLCG1 mutants increased TCR-triggered T cell activation

To determine if the ATLL mutations of PLCG1 promote LAT condensation in T cells, we constructed Jurkat T cell lines stably expressing LAT-mCherry and wild-type or mutant PLCG1 through lentiviral transduction. We kept the endogenous copy of PLCG1 in these cells because these mutations are heterozygous in patients. The Jurkat cells were dropped onto glass coated with OKT3, an anti-CD3 epsilon antibody that activates the TCR signaling. TIRF microscopy revealed the formation of LAT condensates as Jurkat cells spread on the imaging glass (**Fig. 2A**). We found that, consistent with results from the above biochemical reconstitution assay, PLCG1 mutants enhanced LAT condensation in activated Jurkats (**Fig. 2B, 2C**). In addition to the scaffolding function in promoting LAT condensation, two of the PLCG1 mutants S345F and D1165H increased phosphorylation of PLCG1, which is a marker for the activation of PLCG1 (**Fig. 2D, 2E**). These results motivated us to further determined LAT and PLCG1 downstream signaling. We found that Jurkat cells expressing the three mutants showed higher ERK phosphorylation (**Fig. 2D, 2E**) and calcium influx (**Fig. 2F**) as compared to those expressing the wild-type PLCG1.

To determine how PLCG1 mutants affect primary T cell activation, we primed human T cells isolated from healthy donors using dynabeads, and infected these cells with

lentivirus encoding the wild-type or three mutants of PLCG1. T cells expressing the mutants displayed a higher expression of CD69 (**Fig. 2G**), a T cell activation marker, and higher proliferation (**Fig. 2H**), as compared to the wild-type PLCG1. These results were repeated using T cells from a different donor (**Fig. S2A, S2B**). Together, these data showed that PLCG1 mutants promoted TCR signaling transduction and T cell activation in both the Jurkat T cells line and human primary T cells.

Hyperactive PLCG1 was sufficient to trigger T cell activation and cytokine production without TCR engagement in T cell lymphoma line Hut78

To determine how PLCG1 mutants affect signaling in the context of T-cell leukemia and lymphoma, we used Hut78, a human T lymphoma cell line, as a model. Hut78 displayed a signaling signature more similar to that of activated primary T cells than Jurkat cells(Bartelt et al, 2009). We infected Hut78 with lentivirus encoding the wild-type or mutant PLCG1. To determine whether these mutations are sufficient to trigger T cell activation without TCR engagement, we performed the below measurements in the absence of TCR stimuli. We found that even though the expression levels of the mutants were lower than the wild-type PLCG1, an increase in phospho-PLCG1 (pY783, a marker for PLCG1 activation) was observed in S345F and D1165H (**Fig. 3A, 3B**). We also found a higher phosphorylation of ERK in all three mutants and higher expression of Bcl2, an anti-apoptosis protein (**Fig. 3A, 3B**). It is noted that the expression of these ectopically expressed PLCG1 mutants (they contained a GFP tag and migrated more slowly on the gel than the endogenous PLCG1) was much higher than that of the endogenous PLCG1. Therefore, we re-infected Hut78 with lentivirus with a lower titer so

that the ectopically expressed PLCG1 is in a similar level to the endogenous one (**Fig. S3A, S3B**). In this case, we still observed enhanced phospho-PLCG1, phospho-ERK, and Bcl2 in PLCG1 mutants as compared to the wild-type PLCG1 (**Fig. S3A, S3B**).

To systematically determine the intracellular signaling triggered by the PLCG1 mutants, we profiled the key kinase phosphorylation using a human phospho-kinase array kit. We identified a few kinases whose phosphorylation was consistently altered in all three mutants (**Fig. 3C**). These include the enhanced phosphorylation of STAT3, which promotes effector T cell differentiation, enhanced phosphorylation of HSP27, which has an anti-apoptosis function, and reduced phosphorylation of Chk-2, a tumor suppressor (**Fig. 3D**). These signaling outcomes are consistent with the notion that PLCG1 mutants promote cell growth and inhibit cell death.

Cytokine production is one of the key functional consequences of TCR pathway activation. Therefore, we determined the production of IL-2 and TGF-beta, the two signature cytokines in the TCR pathway in PLCG1 mutants. We found a higher level of IL-2 and TGF-beta were released by cells expressing the PLCG1 mutants (**Fig. 3E**). Together, the above data suggested that PLCG1 mutants are sufficient to drive hyperactive PLCG1 signaling; they trigger PLCG1 downstream pathways even in the absence of upstream TCR engagement in Hut78 cells.

Hyperactive PLCG1 signaling induced aggregation of Hut78

During the culture of Hut78 cells, we found that cells expressing the PLCG1 mutants, but not the wild-type, formed cell-cell aggregates (**Fig. 4A**). To determine if this aggregation is mediated by soluble factors secreted or by cell adhesion molecules, we plated plain Hut78 cells in conditioned media obtained from cells expressing the mutant PLCG1. We found that the conditioned media did not induce cell aggregation (**Fig. S4A**), arguing against a mechanism that the cell aggregation was solely mediated by soluble factors. On the other hand, we determined the surface expression of common adhesion molecules and found a significant increase of ICAM-1 expression in Hut78 expressing PLCG1 mutants (**Fig. 4B, 4C**). ICAM-1 is the ligand for integrin LFA-1 on T cell surface. LFA-1 was expressed at a comparable level between cells expressing the wild-type and mutant PLCG1 (**Fig. S4B**). To determine if this ICAM-1-LFA-1 interaction contributes to downstream signaling, we treated Hut78 with antibodies blocking ICAM-1-LFA-1 interactions. Indeed, we find a dose-dependent reduction in ERK phosphorylation (**Fig. 4D**, **4E**) (LFA-1 was shown to activate ERK in T cells(Cassioli et al, 2021; Sharma et al, 2018)). Together, these data suggested that PLCG1 mutants induced cell-cell aggregation in conjugation with ICAM-1-LFA-1 signaling to enhance ERK activation.

Hyperactive PLCG1 conferred Hut78 resistance to HDAC inhibitors

The aforementioned data showed that ATLL-related PLCG1 mutations increased ERK phosphorylation. Previous work showed that KRAS-induced ERK signaling conferred cell resistance to vorinostat, a histone deacetylase (HDAC) inhibitor and FDA-approved drug for treating cutaneous T-cell lymphoma(Wang et al, 2016). Therefore, we determined the sensitivity of Hut78 to HDAC inhibitors. We found that PLCG1 mutations

enhanced cell viability after treatment with vorinostat (**Fig. 5A**); consistently, cells expressing PLCG1 mutants were stained with a lower level of apoptosis marker annexin-V (**Fig. 5B, 5C**). Similar resistance was revealed using other HDAC inhibitors belinostat and panobinostat (**Fig. S5A**).

Because mutations in tumors are usually heterogenous among individual cells, next we determined if PLCG1 mutants cause a bystander resistance in adjacent cells that do not acquire mutants. We mixed plain Hut78 cells with Hut78 cells expressing either wild-type or D1165H PLCG1 tagged with GFP in a 1:1 ratio and treated the cell mixture with vorinostat. We found that, the plain Hut78 cells mixed with cells expressing D1165H showed lower apoptosis as compared to the control group that were mixed with cells expressing wild-type PLCG1 (**Fig. S4C, S4D**). This suggested a bystander resistance induced by PLCG1 mutants. What is the mechanism underlying this bystander resistance? We reasoned that PLCG1 mutants induced the expression of ICAM-1, which can bind LFA-1 on both the plain Hut78 or Hut78 expressing PLCG1 mutants and induce co-aggregation. Indeed, when mixing plain Hut78 (labeled with a far-red dye) with Hut78 expressing either the wild-type or D1165H (labeled with GFP), we found that plain Hut78 cells co-aggregated with cells expressing PLCG1 D1165H (**Fig. S4E, S4F**), suggesting the bystander resistance is mediated through cell-cell interactions.

To explore the mechanism of resistance to HDAC inhibitor, we decided to inhibit ERK and STAT3, which we showed were upregulated in PLCG1 mutants. We found that Hut78 cells expressing D1165H showed a similar cell viability to the wild-type PLCG1 in

the presence of an ERK inhibitor LY3214996 whereas LY3214996 itself did not change cell viability (**Fig. 5D**). In contrast, the STAT3 inhibitor napabucasin did not affect the drug resistance of D1165H (**Fig. S5C**). This suggested that ERK signaling mediates PLCG1 mutants-induced resistance to HDAC inhibitors; inhibiting ERK can reverse the drug resistance to vorinostat.

Hyperactive PLCG1 signaling induced a distinct gene profile from TCR activation

PLCG1 sits in one of the many signaling branches that are triggered downstream of TCR. To determine if the PLCG1 mutants only trigger a branch of TCR signaling or they induce pathways beyond the TCR signaling network, we performed bulk RNA sequencing on Hut78 expressing the wild-type or mutant PLCG1. We also included a group in which cells expressing wild-type PLCG1 were activated by anti-CD3/CD28 antibodies as a conventional way to fully activate TCR. We discovered a total of 227 genes that are upregulated or downregulated in all three mutants (**Fig. 6A and Table S2**). Among the 227 genes, only 64 genes were shared between the mutants and TCR activation group (**Fig. S6 and Table S2)**; the rest 163 genes are uniquely altered in hyperactive PLCG1 group but not the TCR activation one (**Fig. 6B and Table S2**). We performed pathway analysis on these 163 genes and found the top pathways including these related to macrophage activation and cytokine storm (**Fig. 6C**). Unexpectedly, the top upregulated pathway relates to smooth muscle contraction, which contains genes including integrins (e.g. ITGB5 and ITGA1), and smooth muscle actin gamma (ACTG2) (**Fig. 6D**). We further confirmed the high expression of smooth muscle actin α-SMA, the marker of smooth muscle differentiation pathway, in Hut78 expressing PLCG1 mutants

by western blot (**Fig. 6E**). In contrast, the expression of universally present beta actin and gamma actin were similar between the wild-type and mutant PLCG1 (**Fig. 6F**). Together, these results showed hyperactive PLCG1 signaling caused distinct gene expression profile from TCR activation.

Alpha smooth muscle actin-dependent activation of PLCG1 mutants

To determine the regulators of the hyperactive PLCG1 signaling in ATLL mutants, we performed pull-down assays to identify PLCG1-interacting partners. Hut78 cells expressing the GFP-tagged wild-type or mutant PLCG1 were lysed. PLCG1 and binding partners were isolated using anti-GFP antibody coated beads and profiled by SDS-PAGE. We found a few specific bands appeared in the S345F and D1165H but not the WT samples (**Fig. 7A**). These bands were cut out and sent for mass spectrometry analysis. They were identified as myosin heavy chain (around 220 kDa), myosin light chain (around 20 kDa) and actin (around 40 kDa) (Table S3). Because the pull-down of actin is specifically detected in D1165H mutant but not the wild-type PLCG1, and because the expression of alpha-SMA, but not that of beta actin or gamma actin was different between the wild-type and D1165H PLCG1 (**Fig. 6E and 6F**), we reasoned that alpha-SMA is likely to directly interact with PLCG1. Indeed, the recombinant PLCG1 D1165H protein binds to filamentous alpha-SMA protein in an actin co-pelleting assay (**Fig. 7B and 7C**). It is noted that the wild-type PLCG1 can also directly bind alpha-SMA, suggesting the binding to alpha-SMA is not restricted to mutant PLCG1.

To determine how alpha-SMA filaments affect PLCG1 activation in cells, we perturbed actin polymerization in Hut78 using drugs that either depolymerize (latrunculin) or stabilize actin (jasplakinolide). We found a decrease in PLCG1 activation with latrunculin and an increase in activation with jasplakinolide in cells expressing PLCG1 D1165H (**Fig. 7D and 7E**). Together, these data suggested that the smooth muscle actin binds and stimulates the activation of PLCG1.

Discussion

In this manuscript, we revealed that the mutated forms of PLCG1 found in ATLL enhanced pro-survival signaling of T lymphocytes. They enhanced LAT condensation to promote ERK activation. They also increased the expression of ICAM-1, which also promote ERK phosphorylation in neighboring cells through the integrin LFA1. The hyperactive ERK signaling rendered drug resistance to HDAC inhibitor vorinostat. We also discovered that PLCG1 mutants induced the expression of smooth muscle actin (alpha-SMA), which is normally restricted to smooth muscle cells. alpha-SMA directly binds PLCG1 to enhance its phosphorylation and unleash the enzyme activity of PLCG1(**Fig. S7**). Together, our work extensively defined the cellular phenotypes of ATLL-associated PLCG1 mutations and provide an underlying molecular mechanism that explains their capacity to promote oncogenesis.

We exploited three common ATLL-related PLCG1 mutants to investigate hyperactive PLCG1 signaling. Among the three, the R48W mutation led to a mild increase in signaling, S345F showed an intermediate effect, and D1165H induced the strongest

response. These signaling patterns align with their known enzymatic activities and their ability to scaffold LAT condensation. Since these mutations are distributed across different regions of PLCG1, the consistent enhancement of pro-survival signaling, proliferation, and drug resistance observed in all mutants suggests that these phenotypes result from PLCG1 hyperactivation, rather than being specific to individual point mutations.

Vorinostat is an FDA-approved drug for cutaneous T-cell lymphoma. However, the overall response rate is usually below 35%(Zinzani et al, 2016), and the mechanism is still incompletely understood. PLCG1 mutations were frequently discovered in cutaneous T-cel lymphoma(Chang et al, 2018; McGirt et al, 2015; Park et al, 2017; Vaque et al, 2014). Our findings that PLCG1 mutants rendered resistance to vorinostat suggested a mechanism explaining the resistance observed in clinics. Importantly, we showed that the ERK inhibitor can reverse the resistance to vorinostat, suggesting a strategy to improve the anti-tumor efficacy of vorinostat.

TCR-triggered native PLCG1 activation is transient (peaks around 1 min and then decays(Zeng et al, 2021)), which imposes a challenge in identifying components that promotes PLCG1 activation. The hyperactive mutants of PLCG1 enabled a constitutively activated PLCG1 form and provided a handle to identify the regulators of PLCG1 which might be missed in TCR-triggered transient activation. Through a pull-down assay, we identified smooth muscle actin as a positive regulator for handle activation.

We unexpectedly discovered that the expression of PLCG1 mutants induced the gene signature of smooth muscle contraction, which is typically restricted to smooth muscle cells. We showed that the signature gene alpha-SMA is specifically expressed in cells acquiring PLCG1 mutants. Alpha-SMA binds and activates PLCG1. This could form a positive loop to strengthen the hyperactive signaling in PLCG1 mutants.

Methods

The materials used in this study including cell lines, plasmids, antibodies, proteins, and chemicals, are listed in supplementary table1.

Cell culture

HEK293T cells were cultured in DMEM medium (Gibco) supplemented with 10% fetal bovine serum (FBS, Gibco) and 1% Penicillin-Streptomycin-L-Glutamine (PSG, Corning). Jurkat and Hut78 cell lines were maintained in RPMI 1640 medium (Gibco) with 10% FBS and 1% PSG. Cells were cultured at 37℃ in a humidified incubator with 5% CO_2.

Recombinant protein purification

Human LAT (aa 1-233), Sos1 (aa 1117-1319), and Grb2 (aa 1-154) recombinant proteins were purified from BL21 (DE3) bacteria as described in our previous study[3]. Rat PLCG1 (aa 21-1215) WT, as well as PLCG1 R48W, S345F, and D1165H mutant proteins were expressed and purified as previous published protocol(Hajicek et al,

2019). The LAT protein remains an N-terminal His_8 tag, while Sos1, Grb2, and PLCG1 were removed N-terminal purification tags, such as GST and His_6.

The full-length human alpha-SMA gene (aa 1-377) gene was cloned into pET-15b vector and transformed into BL21 (DE3) competent cells to express His_6-ybbR-alpha-SMA. The cells were cultured in LB medium with Ampicillin to an OD_{600} of 0.6-0.8 with shaking and then induced with 0.1 mM IPTG for 6 h at 37℃. After induction, the cells were harvested by centrifugation and resuspended in 20 mM Tris-HCl, pH8.0, 300 mM NaCl, 1 mM TCEP, 10% Glycerol containing protease inhibitor cocktail (Roche). Bacterial cells were lysed using a cell disruptor, and the lysate was treated with 0.5% Triton X-100, 10 μg/ml DNase, and 1 mM $MgCl_2$ with rotation at 4°C for 1 hour, followed by centrifugation at 25,000 rpm for 45 minutes at 4°C. The alpha-SMA recombinant protein, associated with bacterial outer membranes, was pelleted and then solubilized with 0.5% N-Lauroylsarcosine sodium salt (Sigma) in a buffer containing 20 mM Tris-HCl (pH 8.0), 150 mM NaCl, 1 mM TCEP, and 10% glycerol. The soluble fraction was then purified using Ni-NTA beads, washed with buffer containing 20 mM imidazole (20 mM Tris-HCl, pH 8.0, 150 mM NaCl, 1 mM TCEP, 10% glycerol), and eluted with 250 mM imidazole in 20 mM Tris-HCl (pH 8.0), 150 mM NaCl, 1 mM TCEP, and 10% glycerol.

Biochemical reconstitution and FRAP analysis of LAT condensate on supported lipid bilayers

PLCG1-driven LAT condensation on lipid bilayers was performed as described previously[10]. Briefly, 96-well glass-bottom imaging plate was cleaned with 5% Hellmanex III (Sigma) overnight, then washed three times with 5 M NaOH at 50 ℃. The

plate was thoroughly rinsed with ddH2O and PBS. Supported NTA lipid bilayers, for anchoring with his-tagged recombinant protein, were formed by adding 20 μl of small unilamellar vesicles (SUVs) containing 2% DOGS-NTA, 0.1% PEG-5000, and 99.8% POPC lipids (Avanti) to 200 μl PBS in each well, incubating for 1 h at 37℃. Excess SUVs were removed by washing with basic buffer (50 mM HEPES, pH 7.4, 150 mM NaCl, 1 mM TCEP). Lipid bilayers were blocked with freshly prepared clustering buffer (50 mM HEPES, pH 7.4, 150 mM NaCl, 1 mM TCEP, 1 mg/ml BSA) for 30 min at 37℃. His8-tagged pLAT-C3B was then incubated with the bilayers for 3 h, followed by washing with clustering buffer to remove unanchored pLAT. LAT condensation on supported lipid bilayers was triggered by adding PLCG1, Grb2, and Sos1 recombinant proteins, diluted in an oxygen scavenger solution (0.2 mg/ml glucose oxidase, 0.035 mg/ml catalase, 70 mM beta-mercaptoethanol, and 25 mM glucose) in clustering buffer, and incubated for 30 min at 37℃. LAT clusters were imaged using a Nikon Ti2-E inverted fluorescence motorized microscope with a 100x TIRF objective. Cluster was photobleached, and fluorescence recovery was monitored over 5 minutes at 2-second intervals using TIRF microscopy. Clustering and FRAP data were analyzed with ImageJ. The LAT clustering level was quantified using normalized variance (SD^2/mean), where the mean represents the average fluorescence intensity after background subtraction. FRAP half-recovery time and recovery percentage were calculated using GraphPad Prism 10.0.1 software, fitted to a one-phase association model.

Live cell imaging of LAT condensation in Jurkat T cells

The 96-well glass-bottom imaging plate was coated with 100 µl of 5 µg/ml anti-CD3 monoclonal antibody OKT3 (eBioscience) in PBS and incubated overnight at room temperature. Unbound OKT3 antibody was then removed by washing with PBS. The plate was equilibrated in 100 µl of imaging medium, consisting of phenol red-free RPMI medium (Gibco) with 20 mM HEPES, pH7.4. Jurkat T cells expressing LAT-mCherry and PLCG1-GFP were harvested and resuspended in imaging medium. TIRF microscopy was used to capture real-time LAT clustering upon adding 100 µl of 1 million/ml Jurkat cells to the OKT3-coated well at 37℃. Data analysis was performed using ImageJ.

Human primary T cell growth assay

Human peripheral blood mononuclear cells (PBMC) were purchased from Zen-Bio company. Primary T cells were isolated using the EasySepTM human T cell isolation kit (Stemcell technologies) according to the manufacturer's instructions. Primary T cells were co-cultured with Human T-activator CD3/CD28 Dynabeads at a 1:1 ratio in RPMI medium (Gibco) supplemented with 10% FBS, 1% PSG, 10 mM HEPES, pH 7.4 (Gibco), 2 mM L-Glutamine (Gibco), 1x MEM-NEAA (Gibco), 0.55 mM 2-mercaptoethanol (Gibco), and 200 U/ml IL-2 (PeproTech) for 3 days. PLCG1-GFP (WT or mutant) lentivirus vectors (3000 ng) was co-transfected with packaging plasmids pMD2.G (500 ng) and psPAX (500 ng) into 293T cells using 12 µl PEI (Polysciences) in a 6-well plate for 48 h. The lentivirus was then collected and used to infect the primary T cells/Dynabeads mixture in the presence of 5 µg/ml polybrene (Santa cruz biotechnology) by plate centrifugation (800 g, 90 min at 32℃). After 4 days of lentiviral

infection, Dynabeads were removed using a magnetic separator (BioLegend), and the infected primary T cells were rested for 5 days to test the T cell growth.

For the human primary T cell growth assay, 0.25 million/ml T cells were seeded into a 96-well U-bottom plate (Corning) in 200 µl primary T cell culture medium. Cell counts were performed using an automated cell counter (Bio-Rad)

Flow cytometry

Cell surface marker detection in T cells: T cells were collected and washed with PBS and sorting buffer (0.5% BSA, 2 mM EDTA in PBS). The cells were stained with fluorescence conjugated antibody on ice for 30 minutes, then washed with sorting buffer. Stained cells were analyzed using a BD FACS machine, and FlowJo software was used for quantifying the FACS data.

Calcium Flux Monitoring in Jurkat Cells: Jurkat T cells stably expressing the calcium sensor GCaMP6s and either wild-type or mutant PLCG1-GFP were collected and resuspended in RPMI medium without phenol red (Gibco), supplemented with 20 mM HEPES, pH 7.4. The cells were loaded into the FACS machine, where their pre-activation status was recorded at low speed for 1 minute. Subsequently, the cells were activated with 10 µg/ml OKT3 antibody and recorded for an additional 5 minutes at low speed. Calcium signals were captured in the DsRed channel and normalized to the average intensity of the pre-activation status for each group.

Apoptosis Analysis in Hut78 Cells: Vorinostat-treated Hut78 cells were collected and washed with PBS and Annexin V binding buffer (10 mM HEPES, pH 7.4, 140 mM NaCl, 2.5 mM $CaCl_2$). Annexin V (BioLegend) was diluted 1:100 in the binding buffer and used

to stain the cells for 15 minutes at room temperature. The cells were then analyzed directly by FACS without further washing.

Western blot and Phospho-kinase profiling

Jurkat cells were washed with PBS and rested for 30 min at 37℃. The cells were stimulated with 2 µg/ml OKT3 and 2 µg/ml Anti-CD28 antibody (eBioscience) for 2 min at 37℃. SDS-PAGE loading buffer (Bio-Rad) containing protease inhibitors cocktail (Roche) was added to stop the activation and lyse the cells. The cell lysate was boiled for 10 min at 100℃ and then centrifuged at 1,4000 rpm for 5 min. The protein supernatant was loaded into 4-20% gradient gel (Bio-Rad) for SDS-PAGE and subsequently transferred to a PVDF membrane (Bio-Rad). The membrane was blocked with 5% nonfat milk in TBST buffer for 1 h at room temperature. It was then incubated overnight at 4℃ with primary antibodies against PLCG1 (CST), PLCG1 pY783 (CST), pERK1/2 pT202/pY204 (CST), and GAPDH (Biolegend) diluted in 3% BSA TBST buffer. The membrane was washed three times with TBST buffer to remove unbound primary antibodies. The membrane was incubated with horseradish peroxidase (HRP)-conjugated secondary antibody (Thermo Scientific) for 1 h at room temperature. TBST buffer was used to wash out unbound secondary antibody for three times. Enhanced chemiluminescent (ECL) HRP substrate (Thermo Scientific) was applied to the membrane for 3 min and then imaged using a chemiDoc imaging system (Bio-Rad). Image lab (Bio-Rad) was utilized to quantify protein expression.

Hut78 cells stably expressing PLCG1-GFP WT, or the mutant were washed with PBS and lysed using SDS-PAGE loading buffer containing a protease inhibitor cocktail. The remaining steps were conducted as described above. The Proteome Profiler Human

Phospho-Kinase Array Kit (R&D Systems) was used to analyze the phosphorylation of 37 kinases in Hut78 cells, following the manufacturer's instructions.

Enzyme-linked immunosorbent assay (ELISA)

Hut78 cells expressing PLCG1-GFP WT, or the mutant were seeded in 24-well plate at a density of 0.4 million/ml in 500 µl of RPMI cell culture medium and incuabted for 72 h. The cells were spun down, and the supernatant was used for ELISA analysis of IL-2 and latent TGF-beta secretion levels by the kits from Biolegend according to manufacturer's instructions.

Cell aggregation assay

Hut78 cells were seeded in 96-well flat-bottom plate with 0.1 million cells per well in 200 µl of RPMI cell culture medium and incubated for 48 h. The EVOS cell imaging system (Thermo) was used to record cell aggregates at 4x objective.

Cell viability analysis

Hut78 cells were seeded in 96-well plate at a cell density of 0.4 million/ml in 100 µl of RPMI cell culture medium and incubated overnight. Drugs were diluted into 100 µl of RPMI cell culture medium and used to treat the cells for 72 h. Cell counting kit-8 (CCK8, Dojindo) was then added to each well at a volume of 10 µl, followed by a 2 h incubation at 37℃. The optical density at 450 nm (OD450) was recorded by a plate reader (Molecular devices).

Pull-down assay

Hut78 cells expressing PLCG1-GFP WT, or the mutant were washed for three times with PBS and then lysed in 1% Triton X-100 in 20 mM Tris, pH 8.3, 150 mM NaCl buffer containing protease inhibitor cocktail, with vertexing for 30 min at 4℃. The lysate was centrifuged at 1, 5000 rpm for 15 min at 4℃, and the supernatant was collected and quantified for total protein concentration using Bradford assay with Bio-Rad protein assay dye reagent concentrate. MonoMag protein G beads (Ocean nanotech) were washed three times with 0.25% Triton X-100 in 20 mM Tris-HCl, pH 8.3, 150 mM NaCl. The protein G beads, anti-GFP antibody (Invitrogen), and 500 μg of cell lysate were co-incubated with rotation overnight at 4℃. The beads were further washed three times with 0.25% Triton X-100 in 20 mM Tris-HCl, pH 8.3, 150 mM NaCl. The pull-down binding proteins on beads were mixed with loading buffer (Bio-Rad). The beads mixture was loaded into 4-20% gradient gel for SDS-PAGE analysis. Blue safe protein stain (Thermo) reagent was used to stain the gel. The specific band was cut and stored in 1% acetic acid for Mass Spectrometry analysis at the Protein Facility of the Iowa State University Office of Biotechnology.

Actin binding partner spin-down assay

Recombinant alpha-SMA protein was buffer-exchanged to 5 mM Tris-HCl, pH 8.0, 0.2 mM CaCl2, 1 mM TCEP, 1 mM DTT using Cytiva PD SpinTrap G-25 column (GE). Alpha-SMA protein was polymerized into filaments (F-actin) together with Rhodamine muscle actin (Cytoskeleton) by adding 10x polymerization buffer (250 mM Tris-HCl, pH 7.2, 500 mM KCl, pH 8.0, 20 mM MgCl2) and incubating for 1 h at room temperature. The F-actin pellet was spun down at 83,000 g for 30 min in a high-speed centrifuge and

resuspended in 50 mM HEPES, pH 7.4, 150 mM NaCl, 1 mM TCEP. F-actin, PLCG1, and Myosin proteins were co-incubated in 50 µl of 50 mM HEPES, pH 7.4, 150 mM NaCl, 1 mM TCEP for 2 h at room temperature. A high-speed centrifuge was then used to pellet the F-actin binding partners. The supernatant and pellet were loaded into 4-20% gradient gel for SDS-PAGE analysis. Blue safe protein stain (Thermo) reagent was used to stain the gel.

Data availability and statistical analysis

The metadata for RNA-seq data have been submitted to the NCBI GEO database under accession number GSE280396. Unpaired t test was conducted to statistically analyze the differences between two groups using GraphPad Prism version 10.0.1 software. *$p < 0.05$, **$p < 0.01$, ***$p < 0.001$, ns: no significant.

Acknowledgements

We thank Markus Müschen at Yale University for providing Hut78 cells. We thank Diane Krause at Yale University for discussion of the work. X.S. was supported by an American Cancer Society Research Scholar Grant 135926, the Rally Foundation A Collaborative Pediatric Cancer Research Awards Program 22YIC53, the Yale SPORE in skin cancer DRP Award P50 CA121974, the Yale Cancer Center Pilot Award, the Yale DeLuca Pilot Award, the NIGMS MIRA program R35 GM138299, the Gabrielle's Angel Foundation Medical Research Award, the Pershing Square Sohn Prize for Young Investigators in Cancer research, the NCI Exploratory/Developmental Research Grant R21 CA286364, the Human Frontier Science Program Early-Career Research Grant RGY0088/2021, the Yale Liver Center Pilot Award P30 DK034989, the Yale Lion Heart

Pilot Grant, and the NIH Director's Transformative Research Award EB037112. L.Z. was supported by the CRI-Irvington Postdoctoral Fellowship (CRI3516). X.Z. was supported by the Leslie Warner Postdoctoral Fellowship. K.S. was supported by the Daiichi Sankyo Foundation of Life Science Fellowship. N.H. and J.S. acknowledge support from the NIH (R35 GM149299, R01 CA258993, P30 CA016086, and R56 AG083424).

Author contributions

The project was conceptualized by L.Z. and X.S.. L.Z., X.Z., Y.W., K.S., and N.H. conducted experiments and performed data analysis. X.S. and J.S. obtained funding support. X.S. supervised the project. L.Z. and X.S. wrote the manuscript with inputs from all other authors.

Disclosure and competing interests statement

The authors declare that they have no competing interests.

Reference

Ananthanarayanan B, Das S, Rhee SG, Murray D, Cho W (2002) Membrane targeting of C2 domains of phospholipase C-delta isoforms. *J Biol Chem* **277:** 3568-3575

Balagopalan L, Kortum RL, Coussens NP, Barr VA, Samelson LE (2015) The linker for activation of T cells (LAT) signaling hub: from signaling complexes to microclusters. *J Biol Chem* **290:** 26422-26429

Bartelt RR, Cruz-Orcutt N, Collins M, Houtman JC (2009) Comparison of T cell receptor-induced proximal signaling and downstream functions in immortalized and primary T cells. *PLoS One* **4:** e5430

Behjati S, Tarpey PS, Sheldon H, Martincorena I, Van Loo P, Gundem G, Wedge DC, Ramakrishna M, Cooke SL, Pillay N, Vollan HKM, Papaemmanuil E, Koss H, Bunney TD, Hardy C, Joseph OR, Martin S, Mudie L, Butler A, Teague JW, Patil M, Steers G, Cao Y, Gumbs C, Ingram D, Lazar AJ, Little L, Mahadeshwar H, Protopopov A, Al Sannaa GA, Seth S, Song X, Tang J, Zhang J, Ravi V, Torres KE, Khatri B, Halai D, Roxanis I, Baumhoer D, Tirabosco R, Amary MF, Boshoff C, McDermott U, Katan M, Stratton MR, Futreal PA, Flanagan AM, Harris A, Campbell PJ (2014) Recurrent PTPRB and PLCG1 mutations in angiosarcoma. *Nat Genet* **46:** 376-379

Cassioli C, Balint S, Compeer EB, Felce JH, Gamberucci A, Della Bella C, Felce SL, Brunetti J, Valvo S, Pende D, D'Elios MM, Moretta L, Dustin ML, Baldari CT (2021) Increasing LFA-1 Expression Enhances Immune Synapse Architecture and T Cell Receptor Signaling in Jurkat E6.1 Cells. *Front Cell Dev Biol* **9:** 673446

Chang LW, Patrone CC, Yang W, Rabionet R, Gallardo F, Espinet B, Sharma MK, Girardi M, Tensen CP, Vermeer M, Geskin LJ (2018) An Integrated Data Resource for Genomic Analysis of Cutaneous T-Cell Lymphoma. *J Invest Dermatol* **138:** 2681-2683

Chen D, Simons M (2021) Emerging roles of PLCgamma1 in endothelial biology. *Sci Signal* **14**

Courtney AH, Lo WL, Weiss A (2018) TCR Signaling: Mechanisms of Initiation and Propagation. *Trends Biochem Sci* **43:** 108-123

Falasca M, Logan SK, Lehto VP, Baccante G, Lemmon MA, Schlessinger J (1998) Activation of phospholipase C gamma by PI 3-kinase-induced PH domain-mediated membrane targeting. *EMBO J* **17:** 414-422

Gresset A, Hicks SN, Harden TK, Sondek J (2010) Mechanism of phosphorylation-induced activation of phospholipase C-gamma isozymes. *J Biol Chem* **285:** 35836-35847

Hajicek N, Keith NC, Siraliev-Perez E, Temple BR, Huang W, Zhang Q, Harden TK, Sondek J (2019) Structural basis for the activation of PLC-gamma isozymes by phosphorylation and cancer-associated mutations. *Elife* **8**

Huang WYC, Alvarez S, Kondo Y, Lee YK, Chung JK, Lam HYM, Biswas KH, Kuriyan J, Groves JT (2019) A molecular assembly phase transition and kinetic proofreading modulate Ras activation by SOS. *Science* **363:** 1098-1103

Kataoka K, Nagata Y, Kitanaka A, Shiraishi Y, Shimamura T, Yasunaga J, Totoki Y, Chiba K, Sato-Otsubo A, Nagae G, Ishii R, Muto S, Kotani S, Watatani Y, Takeda J, Sanada M, Tanaka H, Suzuki H, Sato Y, Shiozawa Y, Yoshizato T, Yoshida K, Makishima H, Iwanaga M, Ma G, Nosaka K, Hishizawa M, Itonaga H, Imaizumi Y, Munakata W, Ogasawara H, Sato T, Sasai K, Muramoto K, Penova M, Kawaguchi T, Nakamura H, Hama N, Shide K, Kubuki Y, Hidaka T, Kameda T, Nakamaki T, Ishiyama K, Miyawaki S, Yoon SS, Tobinai K, Miyazaki Y, Takaori-Kondo A, Matsuda F, Takeuchi K, Nureki O, Aburatani H, Watanabe T, Shibata T, Matsuoka M, Miyano S, Shimoda K, Ogawa S (2015) Integrated molecular analysis of adult T cell leukemia/lymphoma. *Nat Genet* **47:** 1304-1315

Lomasney JW, Cheng HF, Kobayashi M, King K (2012) Structural basis for calcium and phosphatidylserine regulation of phospholipase C delta1. *Biochemistry* **51:** 2246-2257

McGirt LY, Jia P, Baerenwald DA, Duszynski RJ, Dahlman KB, Zic JA, Zwerner JP, Hucks D, Dave U, Zhao Z, Eischen CM (2015) Whole-genome sequencing reveals oncogenic mutations in mycosis fungoides. *Blood* **126:** 508-519

Park J, Yang J, Wenzel AT, Ramachandran A, Lee WJ, Daniels JC, Kim J, Martinez-Escala E, Amankulor N, Pro B, Guitart J, Mendillo ML, Savas JN, Boggon TJ, Choi J (2017) Genomic analysis of 220 CTCLs identifies a novel recurrent gain-of-function alteration in RLTPR (p.Q575E). *Blood* **130:** 1430-1440

Patel VM, Flanagan CE, Martins M, Jones CL, Butler RM, Woollard WJ, Bakr FS, Yoxall A, Begum N, Katan M, Whittaker SJ, Mitchell TJ (2020) Frequent and Persistent PLCG1

Mutations in Sezary Cells Directly Enhance PLCgamma1 Activity and Stimulate NFkappaB, AP-1, and NFAT Signaling. *J Invest Dermatol* **140:** 380-389 e384

Qi Q, August A (2007) Keeping the (kinase) party going: SLP-76 and ITK dance to the beat. *Sci STKE* **2007:** pe39

Sharma A, Lawry SM, Klein BS, Wang X, Sherer NM, Zumwalde NA, Gumperz JE (2018) LFA-1 Ligation by High-Density ICAM-1 Is Sufficient To Activate IFN-gamma Release by Innate T Lymphocytes. *J Immunol* **201:** 2452-2461

Su X, Ditlev JA, Hui E, Xing W, Banjade S, Okrut J, King DS, Taunton J, Rosen MK, Vale RD (2016) Phase separation of signaling molecules promotes T cell receptor signal transduction. *Science* **352:** 595-599

Su X, Ditlev JA, Rosen MK, Vale RD (2017) Reconstitution of TCR Signaling Using Supported Lipid Bilayers. *Methods Mol Biol* **1584:** 65-76

Tao P, Han X, Wang Q, Wang S, Zhang J, Liu L, Fan X, Liu C, Liu M, Guo L, Lee PY, Aksentijevich I, Zhou Q (2023) A gain-of-function variation in PLCG1 causes a new immune dysregulation disease. *J Allergy Clin Immunol* **152:** 1292-1302

Vaque JP, Gomez-Lopez G, Monsalvez V, Varela I, Martinez N, Perez C, Dominguez O, Grana O, Rodriguez-Peralto JL, Rodriguez-Pinilla SM, Gonzalez-Vela C, Rubio-Camarillo M, Martin-Sanchez E, Pisano DG, Papadavid E, Papadaki T, Requena L, Garcia-Marco JA, Mendez M, Provencio M, Hospital M, Suarez-Massa D, Postigo C, San Segundo D, Lopez-Hoyos M, Ortiz-Romero PL, Piris MA, Sanchez-Beato M (2014) PLCG1 mutations in cutaneous T-cell lymphomas. *Blood* **123:** 2034-2043

Wada J, Rathnayake U, Jenkins LM, Singh A, Mohammadi M, Appella E, Randazzo PA, Samelson LE (2022) In vitro reconstitution reveals cooperative mechanisms of adapter protein-mediated activation of phospholipase C-gamma1 in T cells. *J Biol Chem* **298:** 101680

Wang M, Zhang S, Chuang SS, Ashton-Key M, Ochoa E, Bolli N, Vassiliou G, Gao Z, Du MQ (2017) Angioimmunoblastic T cell lymphoma: novel molecular insights by mutation profiling. *Oncotarget* **8:** 17763-17770

Wang Q, Tan R, Zhu X, Zhang Y, Tan Z, Su B, Li Y (2016) Oncogenic K-ras confers SAHA resistance by up-regulating HDAC6 and c-myc expression. *Oncotarget* **7:** 10064-10072

Zeng L, Palaia I, Saric A, Su X (2021) PLCgamma1 promotes phase separation of T cell signaling components. *J Cell Biol* **220**

Zeng L, Su X (2023) Biomolecular Condensation of SH2 Domain-Containing Proteins on Membranes. *Methods Mol Biol* **2705:** 371-379

Zhang W, Sloan-Lancaster J, Kitchen J, Trible RP, Samelson LE (1998) LAT: the ZAP-70 tyrosine kinase substrate that links T cell receptor to cellular activation. *Cell* **92:** 83-92

Zinzani PL, Bonthapally V, Huebner D, Lutes R, Chi A, Pileri S (2016) Panoptic clinical review of the current and future treatment of relapsed/refractory T-cell lymphomas: Cutaneous T-cell lymphomas. *Crit Rev Oncol Hematol* **99:** 228-240

Figures:

Fig. 1

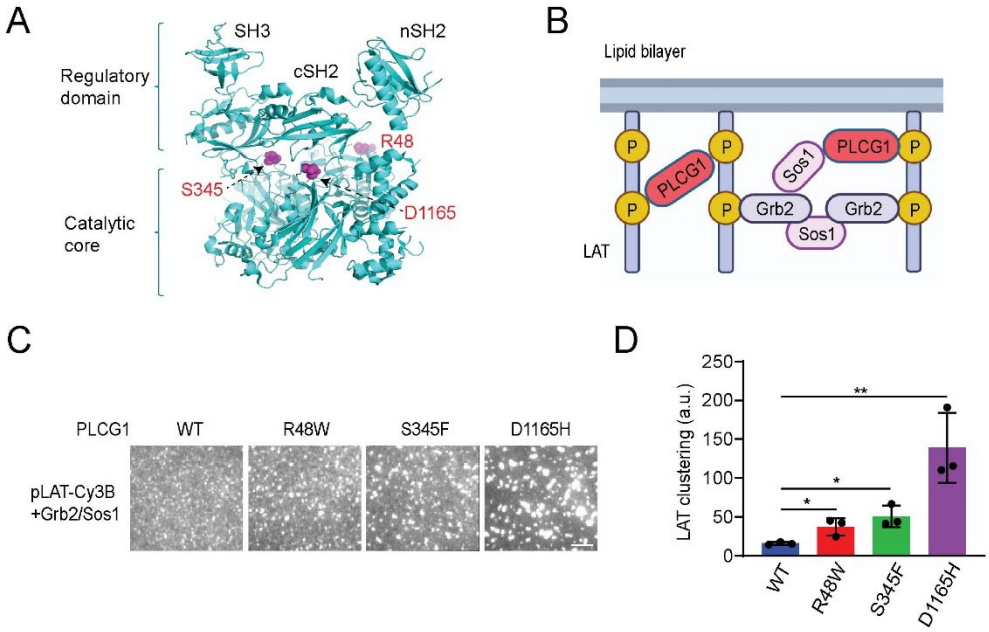

Fig. 1: PLCG1 acquiring ATLL-associated mutations promoted LAT condensation *in vitro*.

(A) Location of the three T-cell leukemia/lymphoma-associated mutations in the structure of PLCG1 (PDB: 6PBC).

(B) Schematics of biochemical reconstitution of LAT condensation on supported lipid bilayers.

(C) TIRF microscopy revealed that PLCG1 mutations enhanced LAT condensation on bilayers at physiological concentrations. Cy3B-labeled LAT at 300 molecules / μm^2 was incubated with 300 nM Sos1, 3,000 nM Grb2 and 50 nM PLCG1 for 0.5 h before imaging. Scale bar: 5 μm.

(D) Quantification of LAT clustering as normalized variation. Shown are mean ± SD.

Unpaired two-tail t-test was used. *$p < 0.05$, **$p < 0.01$.

Fig. 2

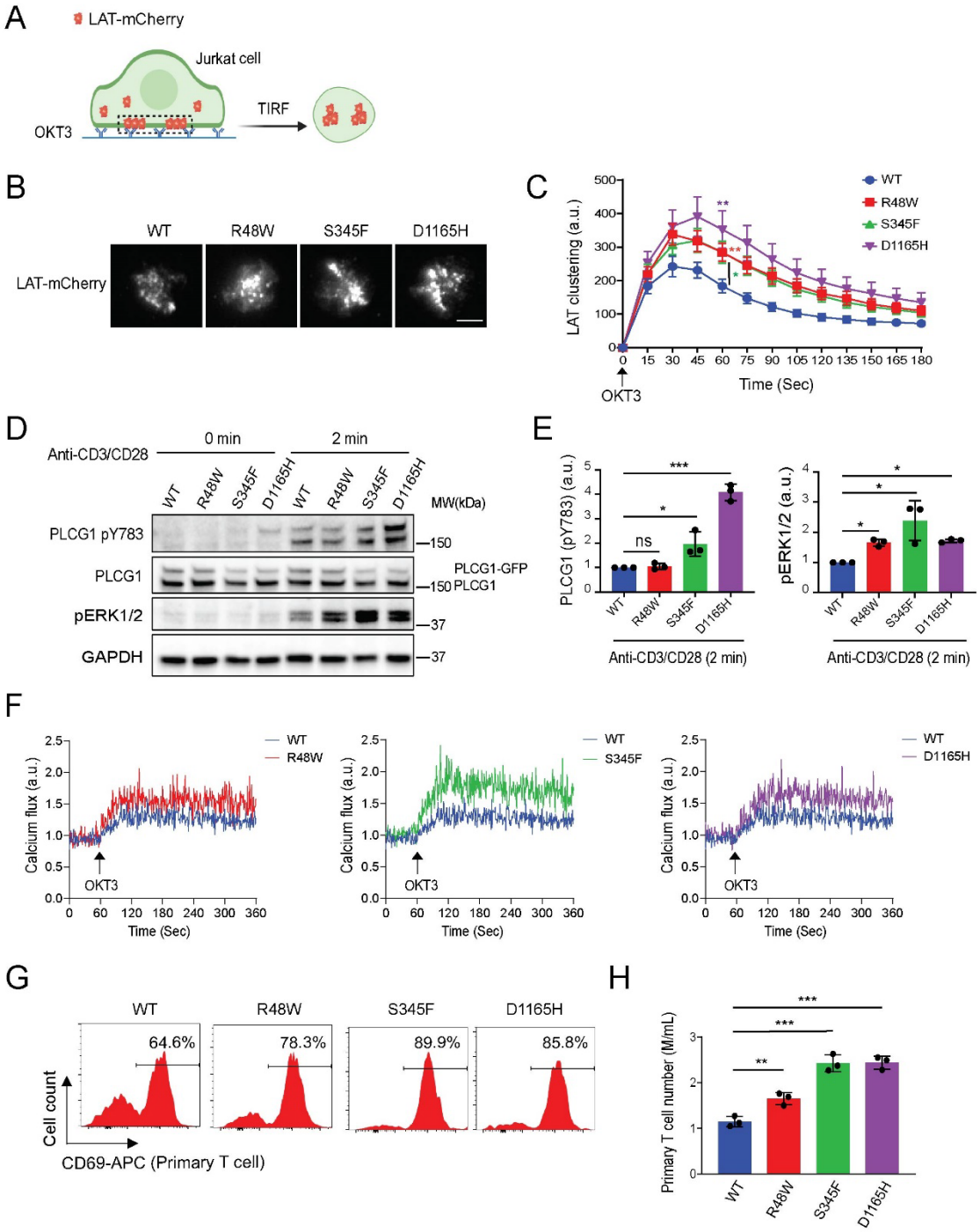

Fig. 2: PLCG1 mutants increased TCR-triggered T cell activation.

(A) Schematics of imaging T cell activation in live cells. Jurkat T cells expressing LAT-mCherry and PLCG1 WT or mutants were plated and activated on OKT3 antibody-coated glass. The formation of LAT condensates on plasma membranes were monitored by time-lapsed TIRF microscopy.

(B) Representative images of Jurkat T cells stimulated with glass-coated OKT3. Images shown were 45 sec after cell landing. Scale bar: 5 μm.

(C) Quantification of LAT clustering during T cell activation. Shown are mean ± SEM. N= 24 to 30 cells. Unpaired two-tail t-test was used for mutation groups compared to WT. *: $p<0.05$, **: $p<0.01$.

(D) Immunoblot analysis of Jurkat T cells harboring PLCG1 WT or indicated mutated variant stimulated with anti-CD3 and anti-CD28 antibodies.

(E) Quantification of (D). Shown are mean ± SD. Unpaired two-tail t-test was used. *$p < 0.05$, ***$p < 0.001$, ns: not significant.

(F) Calcium flux monitored by flow cytometry following TCR activation. Jurkat T cells expressing calcium sensor GCaMP6s and PLCG1 WT or mutation were stimulated by OKT3 antibody and monitored by flow cytometry in a continuous recording mode.

(G) Activation of human primary T cells expressing PLCG1 WT or mutants. The expression of CD69 was determined by flow cytometry 14 days after T cells were infected with lentivirus encoding PLCG1 WT or mutants.

(H) Proliferation of human primary T cells expressing PLCG1 WT or mutants. The cell number was quantified 14 days after T cells were infected with lentivirus encoding PLCG1 WT or mutants. Shown are mean ± SD. $^{**}p < 0.01$, $^{***}p < 0.001$.

Fig. 3

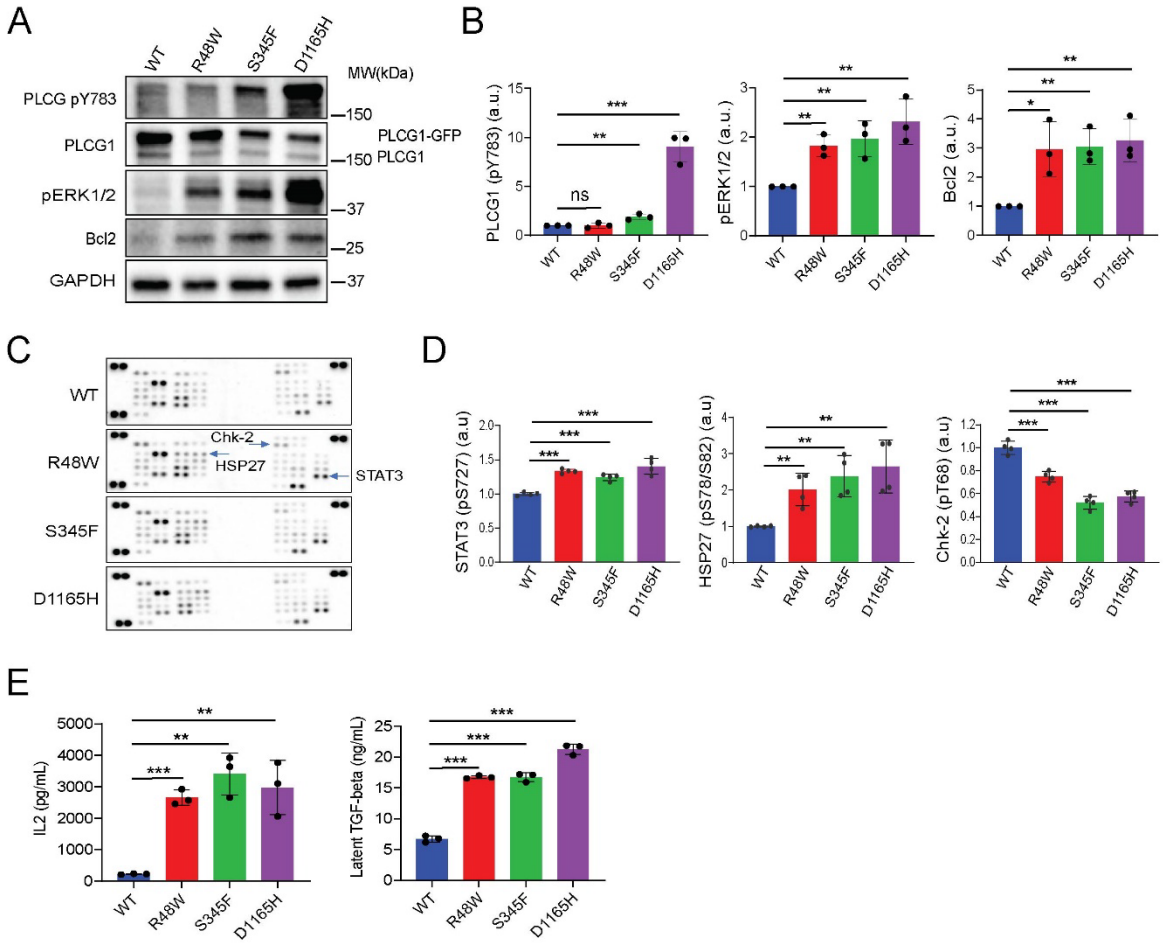

Fig. 3: Hyperactive PLCG1 was sufficient to trigger T cell activation and cytokine production without TCR engagement.

(A) Immunoblot analysis of signaling in Hut78 cells stably expressing PLCG1 WT or mutants (without TCR activation).

(B) Quantification of (A). Shown are mean ± SD. *$p < 0.05$, **$p < 0.01$, ***$p < 0.001$, ns: not significant.

(C) Profiling of protein kinase phosphorylation. Hut78 cells expressing PLCG1 WT or mutations were lysed, and applied to the proteome profiler human phospho-kinase array

kit for analysis. The three kinases with altered phosphorylation were highlighted by blue arrows.

(D) Quantification of the phosphorylation level of kinases. Shown are mean ± SD. $^{**}p < 0.01$, $^{***}p < 0.001$.

(E) ELISA analysis of IL2 and TGF-beta secretion by Hut78 cells. Shown are mean ± SD. $^{**}p < 0.01$, $^{***}p < 0.001$.

Fig. 4

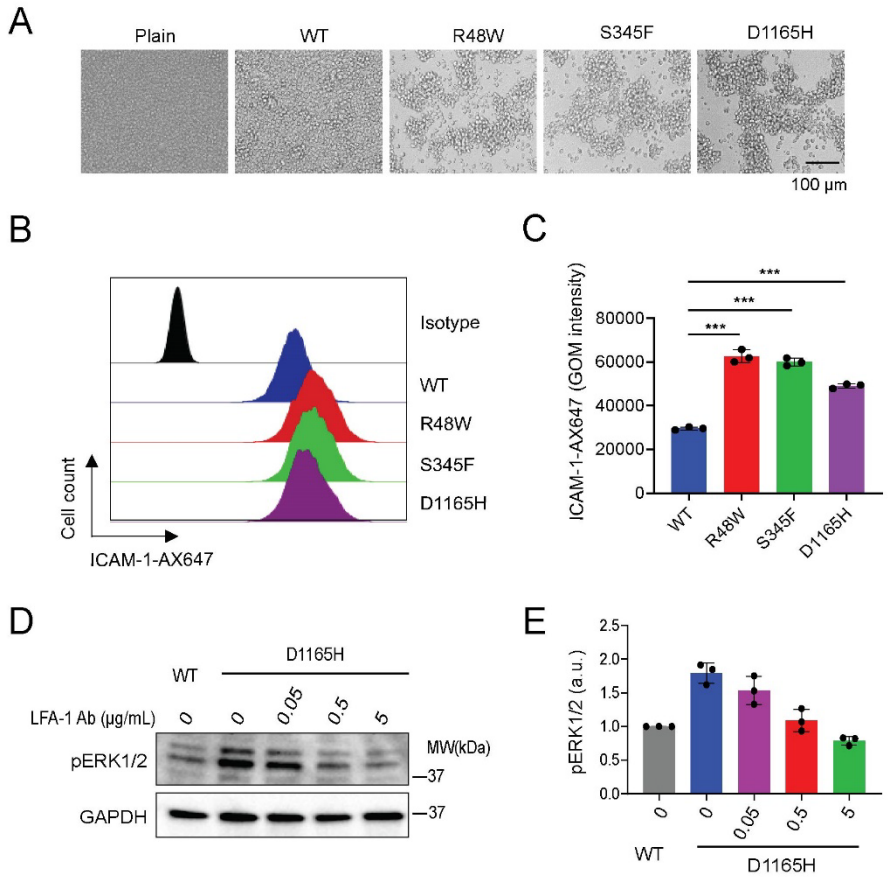

Fig. 4: Hyperactive PLCG1 signaling induced aggregation of Hut78.

(A) Aggregation of Hut78 cells expressing PLCG1 mutants. Scale bar: 100 μm.

(B) Flow cytometry revealed ICAM-1 expression on Hut78 expressing PLCG1 WT or mutants.

(C) Quantification of (B). GOM is geometric mean fluorescence intensity. Shown are mean ± SD. ***$p < 0.001$.

(D) Blocking ICAM-1and LFA-1 interaction inhibited ERK activation. LFA-1 blocking antibody was added to Hut78 expressing PLCG1 D1165H for 36 h.

(E) Quantification of (D). Shown are mean ± SD.

Fig. 5

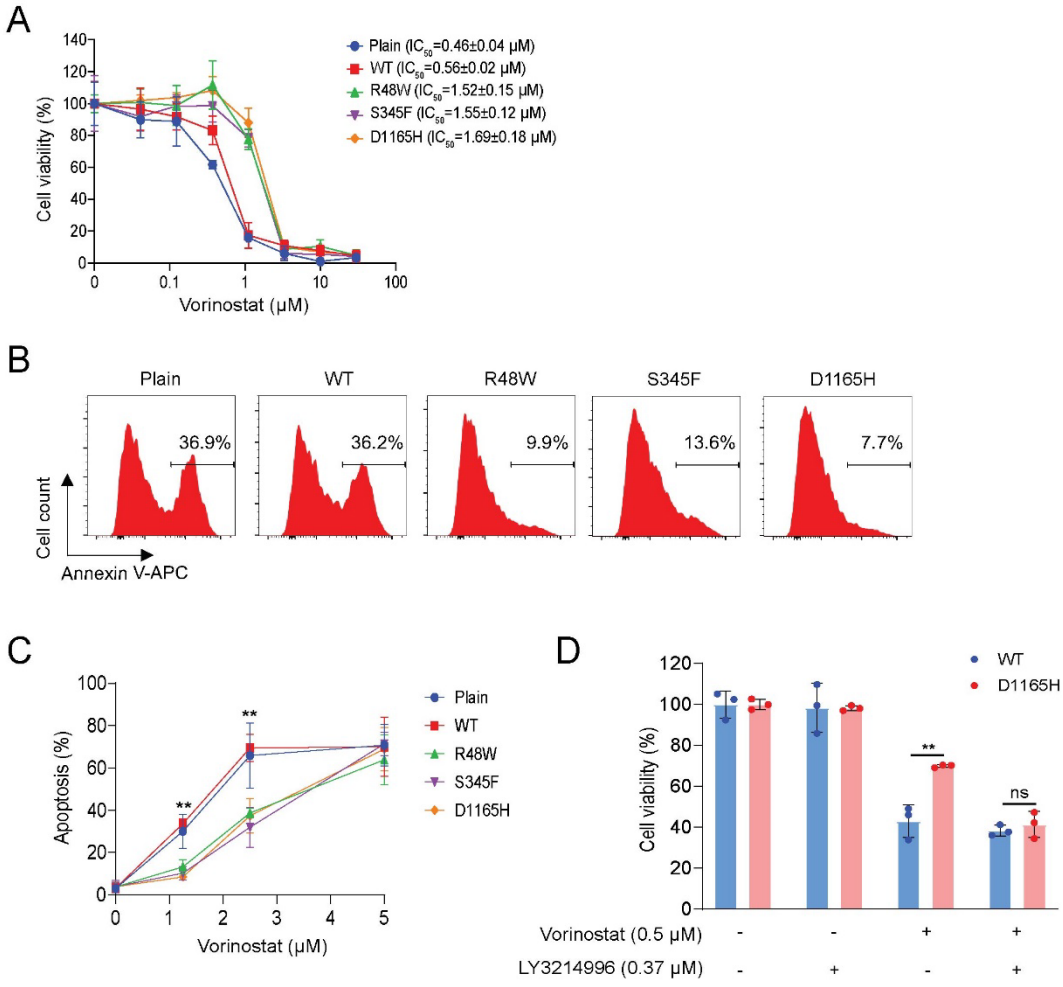

Fig. 5: Hyperactive PLCG1 conferred Hut78 resistance to HDAC inhibitors.

(A) PLCG1 mutations conferred Hut78 resistance to vorinostat. The plain group is Hut78 cells without ectopically expressing PLCG1. The CCK8 assay was used to detect viable cell number after vorinostat treatment for 72 h.

(B) PLCG1 mutations decreased vorinostat-induced apoptosis. Hut78 cells were incubated with 1.25 μM vorinostat for 60 h.

(C) Quantification of (B). Shown are mean ± SD. $^{**}p < 0.01$ (WT vs R48W, S345F, or D116H).

(D) ERK inhibition mitigated vorinostat resistance in Hut78 cells. ERK inhibitor LY3214996 at noncytotoxic concentration 0.37 μM abolished the resistance to vorinostat in Hut78 expressing PLCG1 D1165H. Shown are mean ± SD. $^{**}p < 0.01$, ns: not significant.

Fig. 6

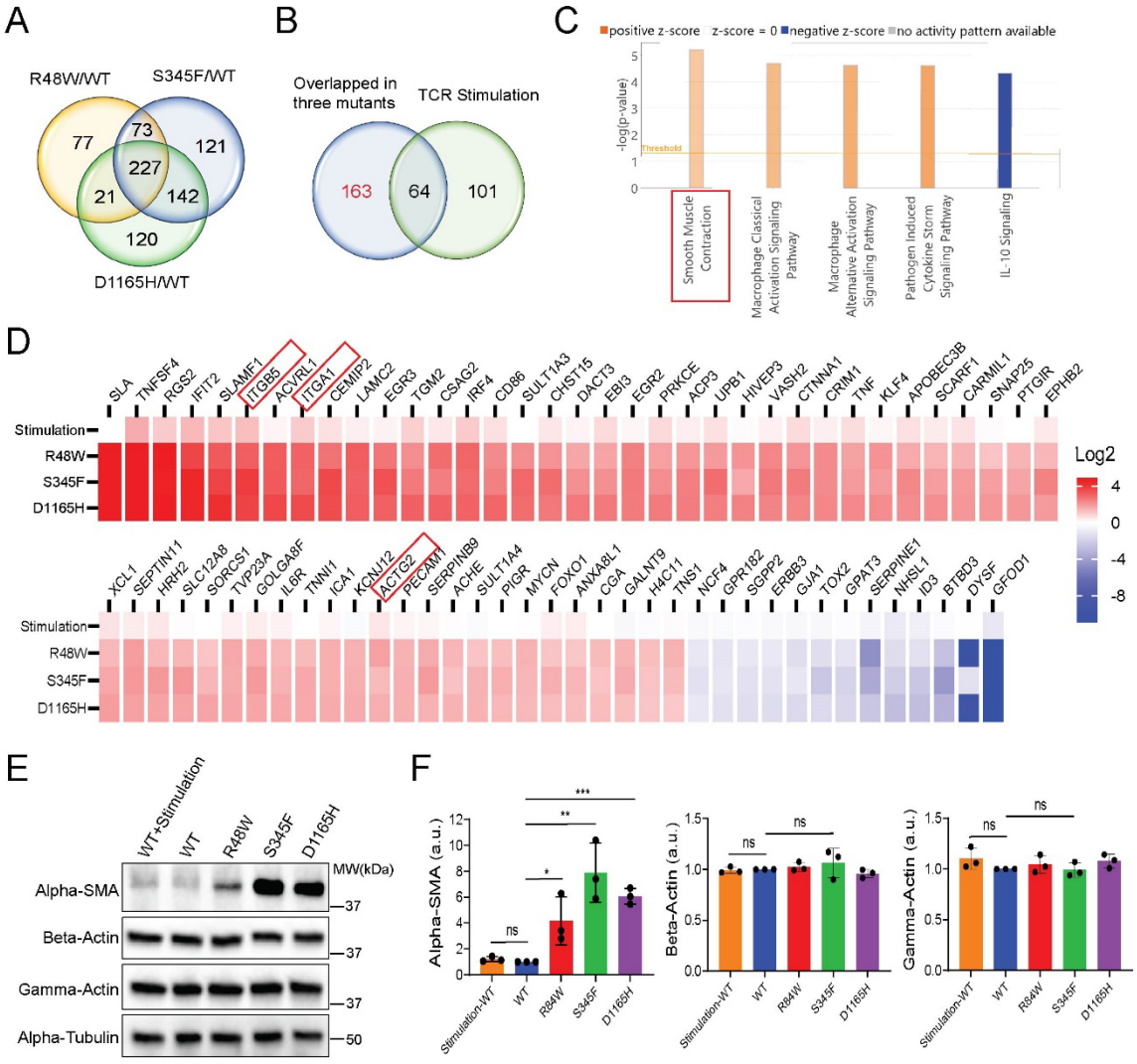

Fig. 6: Hyperactive PLCG1 signaling induces a distinct gene profile from TCR activation.

(A) Venn plot illustrates the gene expression difference in the R48W, S345F and D1165H group as compared to the WT PLCG1. RNA-seq analysis was used to profile gene expression in Hut78 cells expressing WT or mutant PLCG1. Threshold: Log2 fold change>1 and FDR<0.001 when comparing to the WT group.

(B) Comparing gene expression profile between hyperactive PLCG1 signaling and TCR signaling. In the TCR group, Hut78 expressing PLCG1 WT was activated by anti-CD3/CD28 antibodies for 3 days.

(C) Qiagen ingenuity pathway analysis (IPA) revealed pathways enriched in the gene set uniquely triggering by hyperactive PLCG1 signaling but not TCR signaling.

(D) Heatmap illustrated genes uniquely triggered by hyperactive PLCG1 signaling. Shown are the 72 genes which are above 3 folds change of D1165H vs TCR stimulation from the unique 163 genes. Red rectangles indicate genes belong to the smooth muscle contraction pathway. The full list of genes is in supplemental table2.

(E) Immunoblot analysis of actin isoform expression in Hut78 cells. WT+Stimulation: PLCG1 WT was stimulated by anti-CD3/CD28 antibodies for 2 days.

(F) Quantification of the actin expression. Shown are mean ± SD. *$p < 0.05$, **$p < 0.01$, ***$p < 0.001$, ns: not significant.

Fig. 7

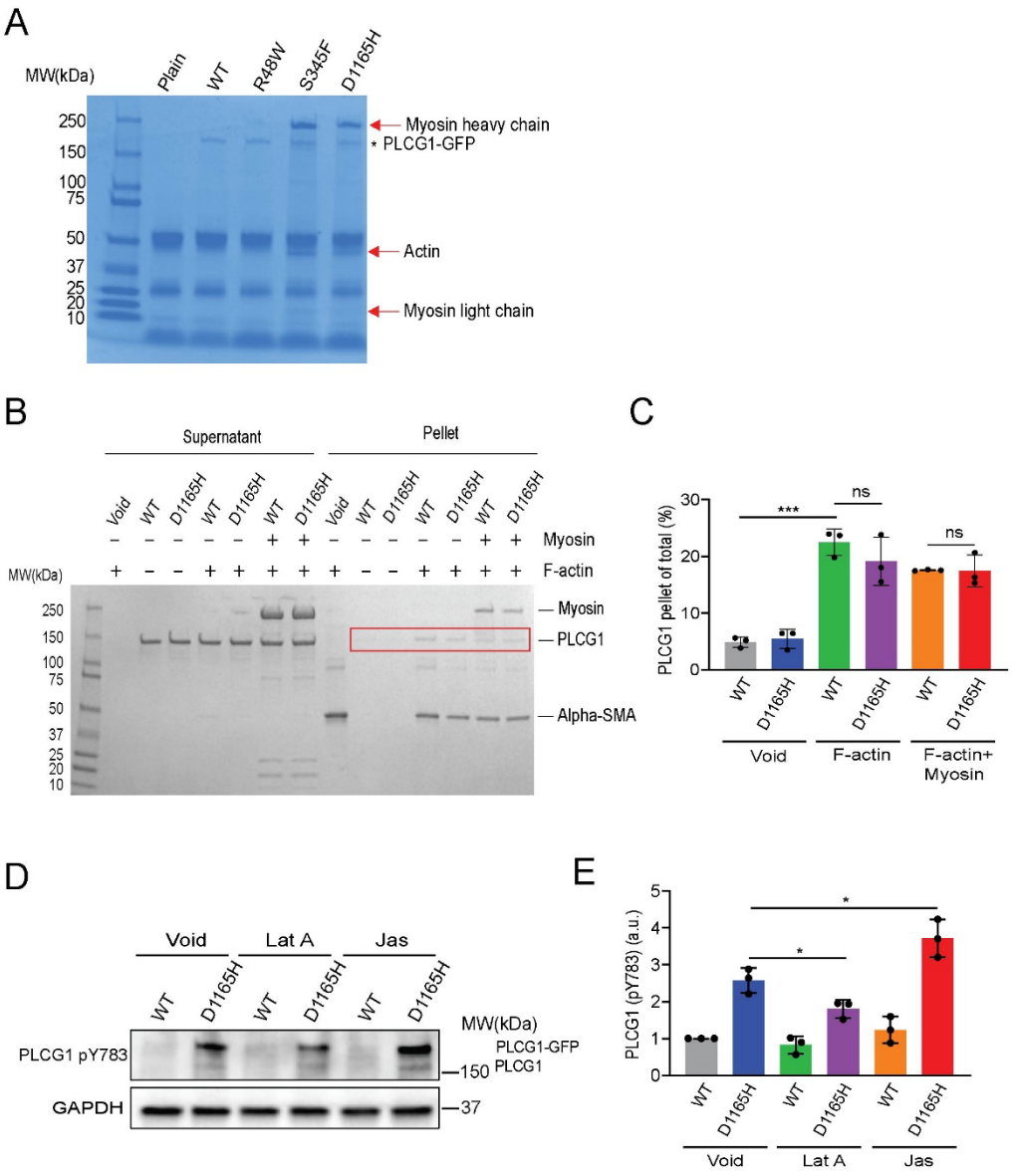

Fig. 7: Alpha smooth muscle actin-dependent activation of ATLL mutations of PLCG1.

(A) Immunoprecipitation assay to identify PLCG1-binding partners. Hut78 cells expressing PLCG1-GFP (WT or mutant) were lysed, pulled down by beads coated with protein G and an anti-GFP antibody-coated, and applied for SDS-PAGE. The specific

bands stained by Coomassie Blue were cut and identified using mass spectrometry. The plain sample is Hut78 cells without exogenously expressed PLCG1.

(B) Pelleting assay to determine the direct interaction between PLCG1 and filamentous actin *in vitro*. Input: 4 μM α-SMA (pre-assembled into filaments), 0.4 μM PLCG1, and 1 μM myosin.

(C) Quantification of PLCG1 binding to F-actin. Shown are mean ± SD. ***$p < 0.001$, ns: not significant.

(D) Regulation of PLCG1 phosphorylation by filamentous actin in Hut78 cells. Actin filaments were destabilized and stabilized with the treatment of 0.5 μM latrunculin A (Lat A) or 0.15 μM jalapinolate (Jas), respectively for 0.5 h.

(E) Quantification of PLCG1 phosphorylation. Shown are mean ± SD. *$p < 0.05$.

Supplementary figures:

Supplementary Fig. S1

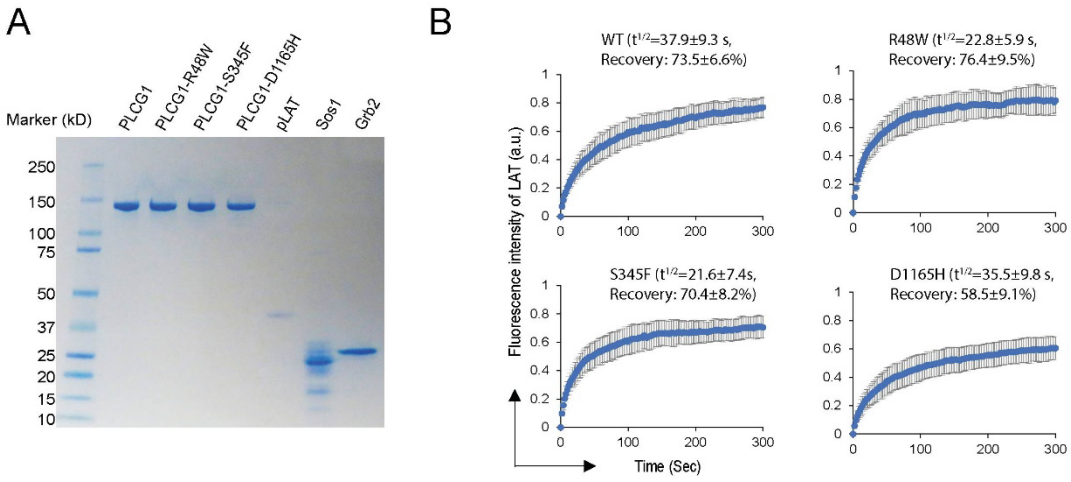

Supplementary Fig. 1: Liquid-like properties of LAT condensate made from PLCG1 mutants.

(A) Recombinant proteins used in this study. The purified proteins were loaded to SDS-PAGE followed by Coomassie Blue staining.

(B) FRAP analysis of LAT condensates.

Supplementary Fig. S2

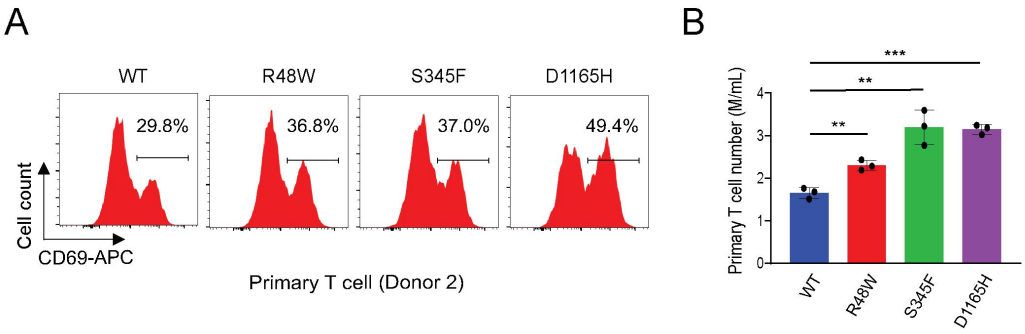

Supplementary Fig. 2: PLCG1 mutations promoted primary T cell activation and growth.

(A) Activation of human primary T cells expressing PLCG1 WT or mutants. The expression of CD69 was determined by flow cytometry 14 days after T cells were infected with lentivirus encoding PLCG1 WT or mutants. This is a repeated experiment using T cells from a different donor than what was used in Figure 2G.

(B) Proliferation of human primary T cells expressing PLCG1 WT or mutants. The cell number was quantified 14 days after T cells were infected with lentivirus encoding PLCG1 WT or mutants. This is a repeated experiment using T cells from a different donor than what was used in Figure 2H. Shown are mean ± SD. $^{**}p < 0.01$, $^{***}p < 0.001$.

Supplementary Fig. S3

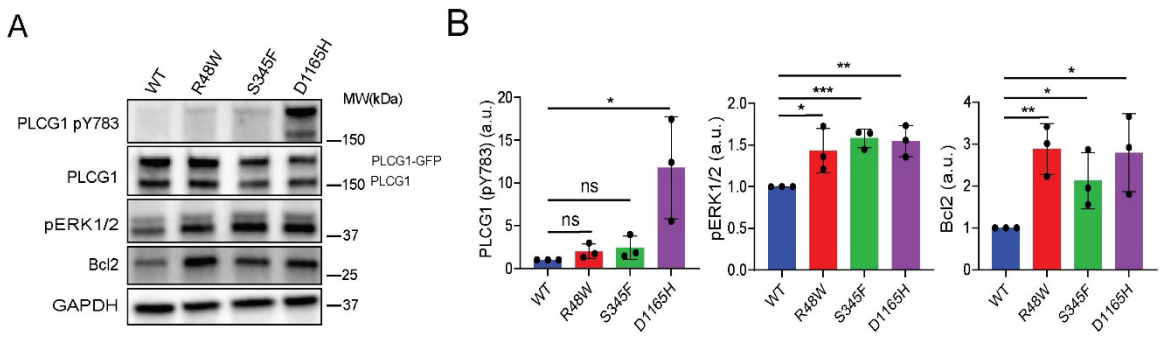

Supplementary Fig. 3: PLCG1 mutants promoted the activation of Hut78 cells.

(A) Immunoblot analysis of signaling in Hut78 cells ectopically expressing GFP-tagged PLCG1 WT or mutants (without TCR activation). Low-titer virus was used so that PLCG1 WT or mutants were expressed at a similar level to the endogenous PLCG1.

(B) Quantification of (A). Shown are mean ± SD. *$p < 0.05$, **$p < 0.01$, ***$p < 0.001$, ns: not significant.

Supplementary Fig. S4

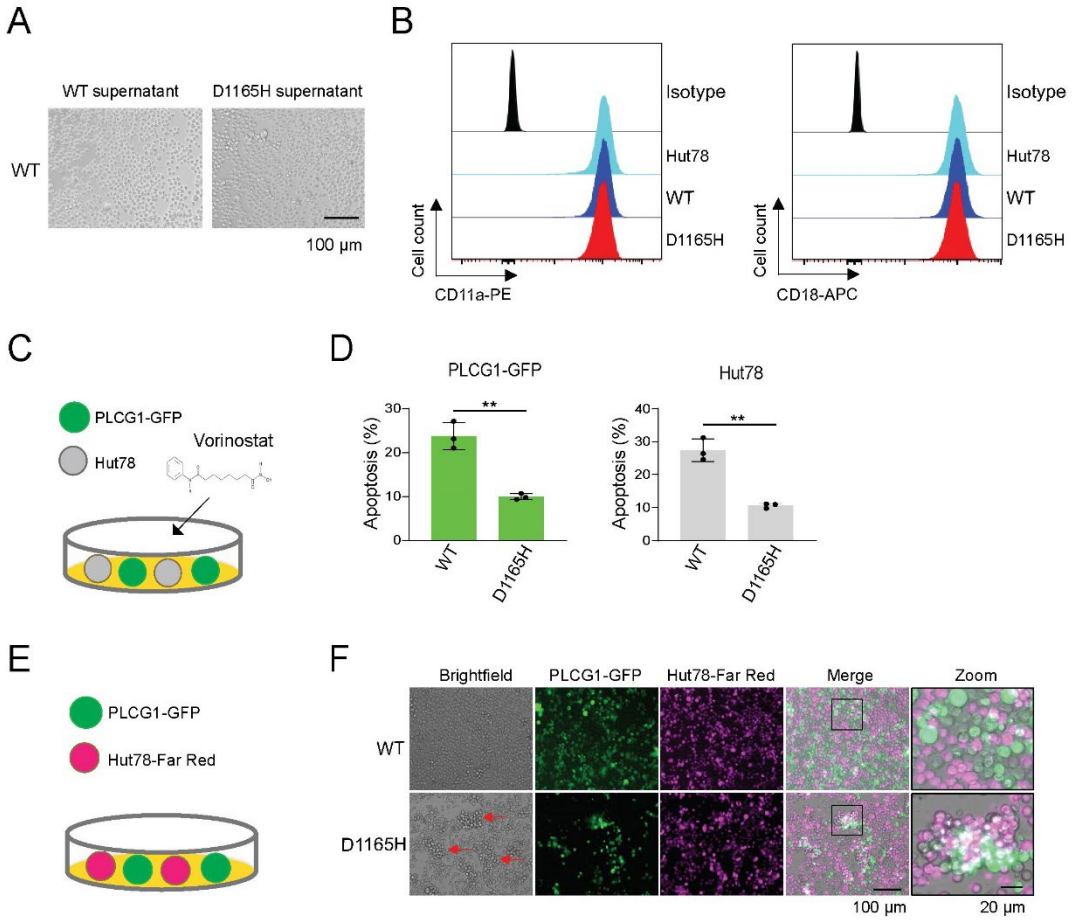

Supplementary Fig. 4: PLCG1 mutations induced bystander resistance to vorinostat.

(A) Conditioned media from Hut78 cells expressing D1165H did not induced cell aggregation. Hut78 cells expressing PLCG1 WT were cultured in supernatant from Hut78 cells expressing the WT or D1165H PLCG1 for 2 days.

(B) The expression of LFA-1 (Two subunits, CD11a and CD18) on the cell surface of Hut78 was detected by flow cytometry.

(C) Schematics of the co-culture assay with vorinostat treatment. Plain Hut78 cells (grey) were co-cultured with Hut78 cells expressing PLCG1-GFP WT or D1165H in a 1:1 ratio for 1 day, and then treated with 1 μM vorinostat for 48 h before being analyzed for apoptosis marker.

(D) Hut78 cells expressing PLCG1 D1165H protected the neighboring plain Hut78 cells from vorinostat-induced apoptosis. Hut78 cells expressing PLCG1 WT or D1165H were cocultured with plain Hut78 cells at 1:1 ratio. The apoptosis level, as indicated by annexin V staining, was determined by flow cytometry. Shown are mean ± SD. $^{**}p < 0.01$.

(E) Schematics of co-culture assay. Hut78 cells harboring PLCG1 WT or D1165H were co-cultured with Far-red dye-labeled plain Hut78 cells at 1:1 ratio.

(F) Plain Hut78 cells co-aggregated with Hut78 expressing D1165H. Red arrow indicates larger cell aggregate. Scale bar: 100 μm. An enlarged inset is shown on the right. Scale bar: 20 μm.

Supplementary Fig. S5

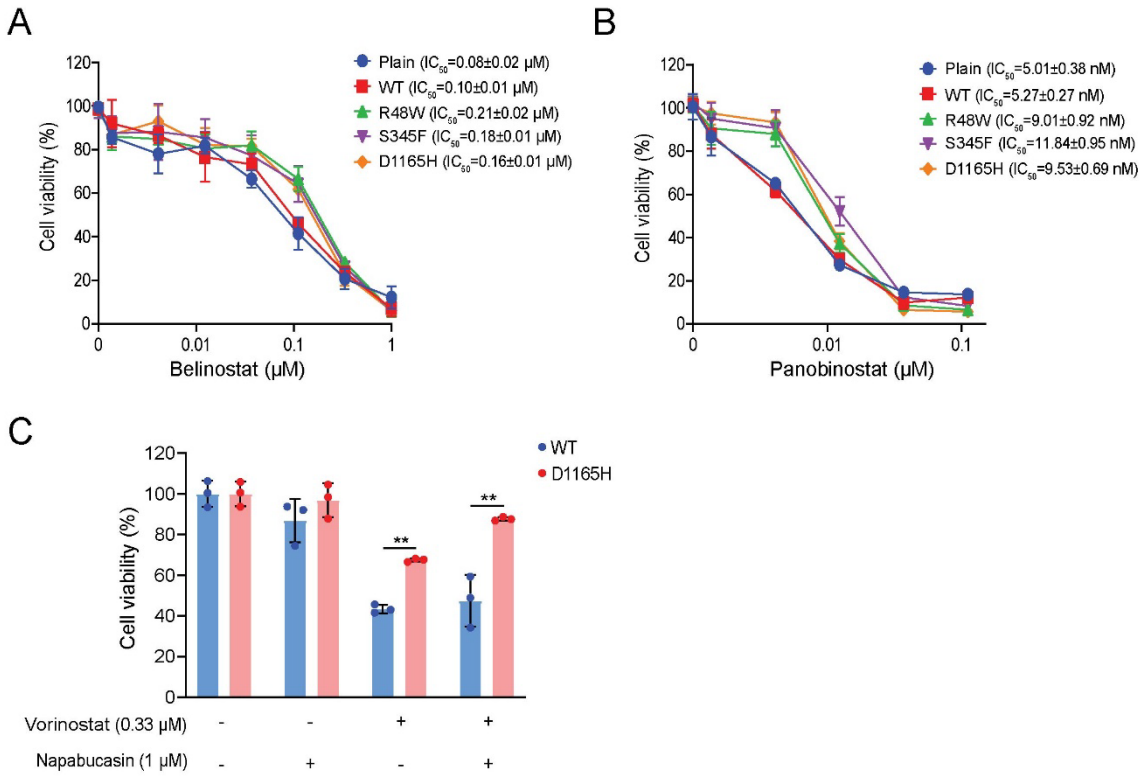

Supplementary Fig. 5: PLCG1 mutations conferred Hut78 resistance to HDAC inhibitors.

(A) PLCG1 mutations conferred Hut78 resistance to belinostat. The plain group is Hut78 cells without ectopically expressed PLCG1. The CCK8 assay was used to detect viable cell number after belinostat treatment for 72 h.

(B) PLCG1 mutations conferred Hut78 resistance to panobionostat. The plain group is Hut78 cells without ectopically expressed PLCG1. The CCK8 assay was used to detect viable cell number after panobinostat treatment for 72 h.

(C) STAT3 inhibitor napabucasin did not affect resistance to vorinostat. Shown are mean ± SD. $^{**}p < 0.01$.

Supplementary Fig. S6

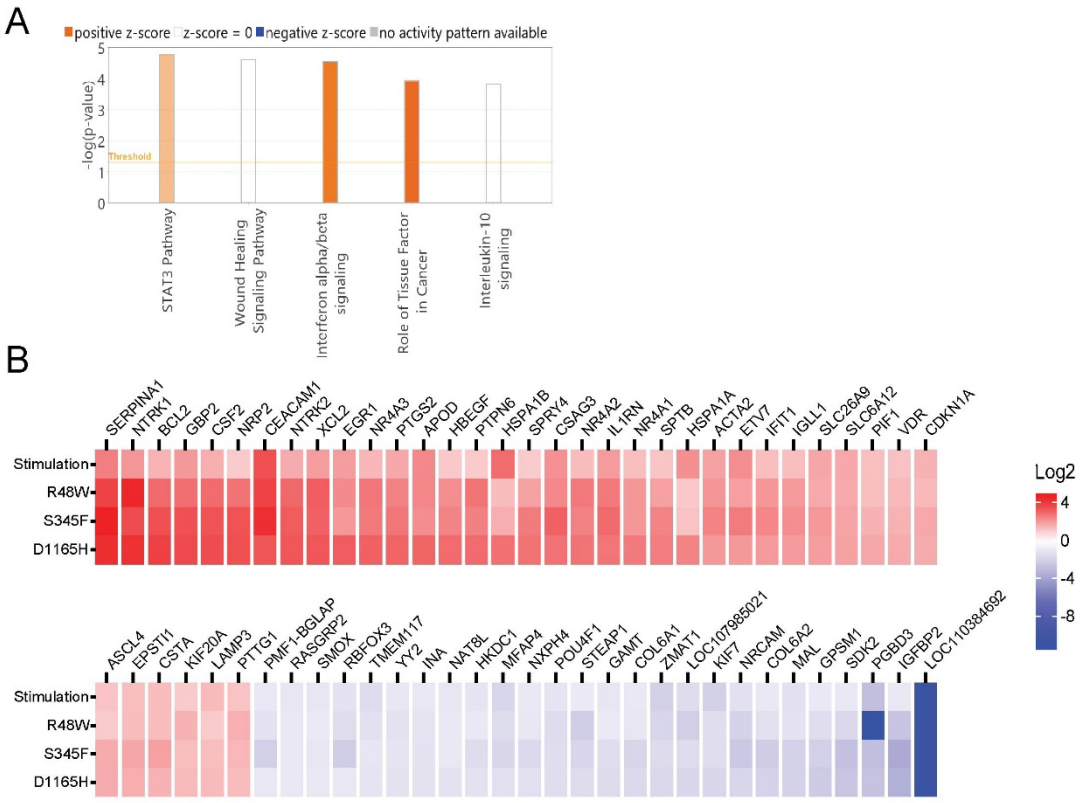

Supplementary Fig. 6: Overlapped genes between hyperactive PLCG1 signaling and TCR signaling.

(A) Qiagen ingenuity pathway analysis (IPA) showed pathways enriched in overlapping genes between hyperactive PLCG1 signaling and TCR signaling.

(B) Heatmap illustrated genes overlapped between hyperactive PLCG1 signaling and TCR signaling. The full list of genes is in supplemental table 2.

Supplementary Fig. S7

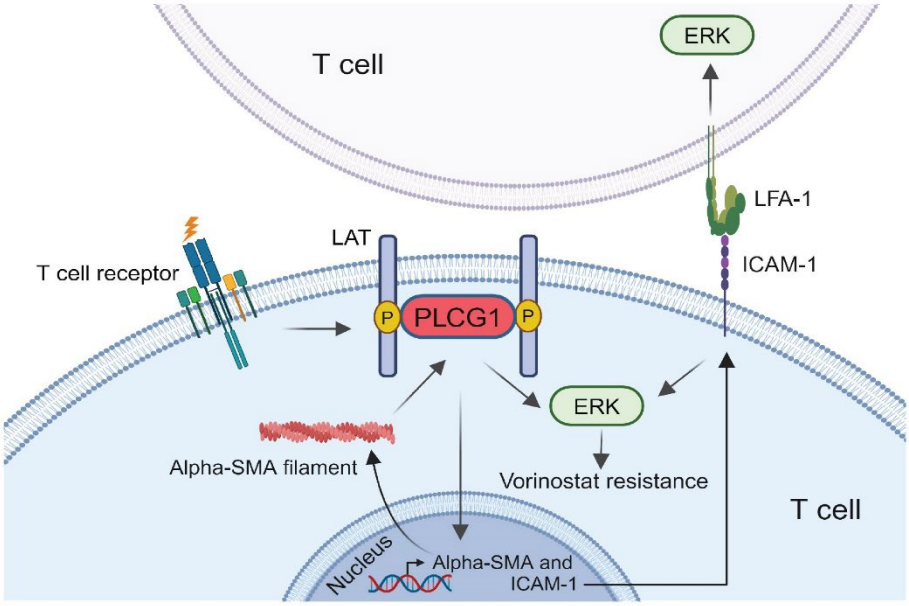

Supplementary Fig. 7: Mechanisms and consequences of hyperactive PLCG1 signaling triggered by T-cell leukemia/lymphoma associated mutations.

Supplementary Table1. Reagents used in this study.

Supplementary Table2. A) The list of 227 genes altered in all three mutants (R48W, S345F, D1165H) as compared to WT, related to Figure 6A. **B)** The list of163 genes altered only in PLCG1 mutants but not in TCR stimulation, related to Figure 6D. **C)** The list of 64 genes altered both in PLCG1 mutants and TCR stimulation, related to Figure S6B.

Supplementary Table3: Mass spectrometry analysis of components specifically interacting with PLCG1 D1165H identified in the pull-down assay in Fig7A.

Reagent type	Designation
Cell line	HEK293T
Cell line	Jurkat T cell E6.1
Cell line	Hut78
Plasmid	pMD2.G
Plasmid	psPAX
Plasmid	pHR-PLCG1-sfGFP
Plasmid	pHR-PLCG1 R48W-sfGFP
Plasmid	pHR-PLCG1 S345F-sfGFP
Plasmid	pHR-PLCG1 D1165H-sfGFP
Plasmid	pET15b_His6-Thrombin-ybbR-alpha-SMA
Antibody	Anti-CD3
Antibody	Anti-CD28
Antibody	APC Anti-CD69
Antibody	Alex Fluor647 Anti-CD54
Antibody	Anti-pERK
Antibody	Anti-PLCG1
Antibody	Anti-PLCG1 pY783
Antibody	Anti-alpha-SMA
Antibody	Anti-beta-actin
Antibody	Anti-gama-actin
Antibody	Anti-GAPDH
Antibody	Anti-Mouse IgG
Antibody	Anti-Rabbit IgG
Antibody	Anti-GFP
Antibody	Anti-CD18
Antibody	APC-Anti-CD18
Antibody	PE-Anti-CD11a
Protein	Rhodamine-actin
Protein	BSA
Beads	Dynabeads
Beads	Protein G Beads
Chemical	Vorinostat
Chemical	Belinostat
Chemical	Panobinostat
Chemical	LY3214996
Chemical	Napabucasin

Source or reference

UCSF
UCSF
Müschen lab at Yale
Su Lab at Yale (XSB395)
Su Lab at Yale (XSB396)
This study (XSB434)
This study (XSB434)
This study (XSB770)
This study (LZB135)
This study (LZB176)
eBioscience
eBioscience
Biolegend
Biolegend
Cell signaling
Cell signaling
Cell signaling
R&D Systems
Cell signaling
Proteintech
Biolegend
Invitrogen
Invitrogen
Invitrogen
Biolegend
Biolegend
Biolegend
Cytoskeleton
Sigma
Thermo
Ocean NanoTech
Cayman chemical
Cayman chemical
Cayman chemical
Cayman chemical
Cayman chemical

Additional information

Lentivirus package
Stable expression cell line construction
Stable expression cell line construction
Viral packaging, Plasmid
Viral packaging, Plasmid
Lentiviral vector. Bovine PLCG1 (UniProt: P08487, aa: 1-1291) fused with an sfGFP tag.
Lentiviral vector. Bovine PLCG1 (UniProt: P08487, aa: 1-1291, R48W) fused with an sfGFP tag.
Lentiviral vector. Bovine PLCG1 (UniProt: P08487, aa: 1-1291, S345F) fused with an sfGFP tag.
Lentiviral vector. Bovine PLCG1 (UniProt: P08487, aa: 1-1291, D1165H) fused with an sfGFP tag.
Protein expression vector. His6-Thrombin-ybbR-alpha SMA (UniProt: P62736, aa: 1-377)
CD3 Monoclonal Antibody (OKT3), Cat#16-0037-85
Cat#16-0289-85
Cat# 310910
ICAM-1 staining Antibody. Cat# 353113
Phospho-p44/42 MAPK (Erk1/2) (Thr202/Tyr204), Cat#9101, WB (1: 2000)
Cat#5690, WB (1: 2000)
Cat#2821, WB (1: 2000)
Cat#MAB1420, WB (1: 5000)
Cat#3700, WB (1: 5000)
Cat#11227-1-AP, WB (1: 5000)
Cat#649202, WB (1: 5000)
Goat anti-Mouse IgG (H+L) Secondary Antibody, Cat#31430, WB (1: 15000)
Goat anti-Rabbit IgG (H+L) Secondary Antibody, Cat#31460, WB (1: 10000)
Cat#A11122, Pull down assay (2 µl per group)
Cat#302102, Blocking antibody for LFA-1
Cat#373405, Detection antibody
Cat#350606, Detection antibody
Cat#AR05-B.
Cat#A9647-100G.
Cat#11132D. Human primary T cells activation.
Cat#MGP3000-002. Pull down assay (50 µl per group)
Cat#10009929
Cat#34084
Cat#13280
Cat#27936
Cat#22255

Gene ID	Gene Symb	Type	log2 (D116	FDR (D116	log2 (R48W	FDR (R48W	log2 (S345I	FDR (S345F/ WT)
6818	'SULT1A3'	mRNA	13.94224	1.91E-46	14.21682	4.62E-55	13.02462	2.36E-24
5739	'PTGIR'	mRNA	12.00141	4.16E-12	11.28771	2.76E-07	12.3443	2.85E-15
7135	'TNNI1'	mRNA	10.55075	0.000119	11.03617	3.61E-06	10.89178	9.29E-06
114815	'SORCS1'	mRNA	10.55075	0.000119	10.89178	1.29E-05	10.22882	0.000859
6503	'SLA'	mRNA	6.247928	8.12E-21	5.554589	3.54E-12	6	2.71E-17
1081	'CGA'	mRNA	5.087463	7.21E-09	5.672425	2.74E-13	4.754888	6.49E-07
8291	'DYSF'	mRNA	4.620586	1.8E-29	4.510962	3.17E-26	4.137504	1.04E-19
5284	'PIGR'	mRNA	4.584963	3.95E-06	4.754888	9.79E-07	5.357552	8.88E-11
4613	'MYCN'	mRNA	4.417853	8.94E-40	3.70044	7.28E-21	4.434628	3.96E-40
5265	'SERPINA1'	mRNA	4.25214	1.15E-77	3.736966	4.88E-48	4.709658	4.9E-113
59269	'HIVEP3'	mRNA	4.251225	3.9E-99	3.217905	1.26E-37	3.76184	3.42E-64
4914	'NTRK1'	mRNA	4.149747	9.21E-32	4.426265	5.35E-39	3.539159	1.56E-18
43	'ACHE'	mRNA	3.807355	2.32E-06	3.321928	0.000345	3.523562	4.64E-05
596	'BCL2'	mRNA	3.786596	8.93E-72	2.85599	2.63E-28	3.443607	4.8E-52
84561	'SLC12A8'	mRNA	3.719892	4.92E-46	3.11221	3.71E-25	3.855052	1.16E-51
6616	'SNAP25'	mRNA	3.628031	1.51E-27	3.212994	3.74E-18	3.254814	2.06E-19
94	'ACVRL1'	mRNA	3.564785	1.92E-14	3.459432	9.72E-13	3.736966	1.02E-16
2634	'GBP2'	mRNA	3.559276	4.3E-198	2.777961	1.16E-87	3.42508	2.5E-173
1959	'EGR2'	mRNA	3.558587	1.22E-53	3.031027	3.18E-31	2.976284	2.27E-30
22903	'BTBD3'	mRNA	3.523562	8.08E-23	2.722466	3.21E-10	3.596935	2.93E-24
1437	'CSF2'	mRNA	3.510962	1.12E-44	2.877744	2.81E-23	3.364572	1.04E-38
9314	'KLF4'	mRNA	3.485427	2.55E-11	2.847997	3.8E-06	3.608809	1.49E-12
8828	'NRP2'	mRNA	3.447726	1.99E-94	2.722466	7.05E-44	3.384664	2.46E-88
634	'CEACAM1'	mRNA	3.321928	0.000243	3.754888	6.65E-06	4.209453	1.07E-08
4915	'NTRK2'	mRNA	3.306161	2.54E-84	2.927649	9.2E-56	3.211148	2.55E-76
6846	'XCL2'	mRNA	3.299751	1.9E-107	3.169925	1.6E-91	3.041249	2.45E-82
1960	'EGR3'	mRNA	3.273018	4.02E-11	3.169925	8.79E-10	2.77259	5.94E-07
7145	'TNS1'	mRNA	3.25634	4.09E-16	3.289507	4.47E-16	3.544321	7.12E-21
147906	'DACT3'	mRNA	3.201634	8.4E-09	2.321928	0.000943	2.887525	1.39E-06
1958	'EGR1'	mRNA	3.179324	9.01E-28	2.270089	2.79E-10	1.978626	1.41E-07
54438	'GFOD1'	mRNA	3.169925	5.52E-07	3.169925	9.69E-07	3.044394	3.19E-06
3918	'LAMC2'	mRNA	3.123382	3.34E-11	2.836501	3.13E-08	3.237039	2.19E-12
84803	'GPAT3'	mRNA	3.087463	1.69E-06	2.754888	0.000117	2.954196	9.52E-06
8013	'NR4A3'	mRNA	3.058894	1.21E-34	2.662965	3.75E-22	2.554589	2.62E-20
79805	'VASH2'	mRNA	3.058894	2.27E-13	2.63743	1.67E-08	3.415037	1.48E-18
5272	'SERPINB9'	mRNA	3.056931	3.1E-151	2.195856	3.19E-55	2.553362	1.9E-87
3382	'ICA1'	mRNA	3.044394	8.57E-12	2.83289	2.83E-09	2.459432	1.32E-06
55	'ACP3'	mRNA	3.037089	6.78E-34	3	1.49E-31	2.874469	1.55E-28
5743	'PTGS2'	mRNA	3.003915	1.1E-124	2.398279	1.21E-61	2.658832	1.14E-85
347	'APOD'	mRNA	2.974005	9.68E-10	2.321928	6.08E-05	2.192645	0.000171
130367	'SGPP2'	mRNA	2.969626	3.88E-16	2.247928	2.68E-07	2.437405	2.71E-09
1839	'HBEGF'	mRNA	2.867362	1.1E-43	2.191426	1.42E-19	2.383004	1.81E-25
5777	'PTPN6'	mRNA	2.846087	1.1E-120	2.671617	2.59E-96	2.443101	1.74E-76
1.03E+08	'CSAG2'	mRNA	2.835513	2.93E-23	2.331485	5.86E-13	3.08883	9.25E-30
51232	'CRIM1'	mRNA	2.834576	1.83E-17	2.180572	2.88E-08	2.95109	1.62E-19
3304	'HSPA1B'	mRNA	2.745754	0	1.2881	8.48E-88	1.528541	1.1E-141
81848	'SPRY4'	mRNA	2.727315	1.01E-45	1.802768	3.35E-14	2.513771	7.62E-36

389903	'CSAG3'	mRNA	2.699672	1.98E-48	2.276234	1.11E-28	3.06778	1.01E-70
4929	'NR4A2'	mRNA	2.685566	2.66E-29	2.584963	2.8E-25	2.405992	2.45E-21
5175	'PECAM1'	mRNA	2.678072	1.38E-19	2.432959	2.02E-14	2.837943	5.37E-23
23670	'CEMIP2'	mRNA	2.678072	1.85E-05	2.847997	3.8E-06	2.584963	5.68E-05
3557	'IL1RN'	mRNA	2.63005	1.66E-19	2.561879	1.96E-17	2.883807	2.75E-25
3570	'IL6R'	mRNA	2.600492	8.41E-68	2.059643	7.46E-34	2.836501	5.62E-87
51363	'CHST15'	mRNA	2.584963	7.92E-41	1.702799	7.76E-13	2.145851	3.6E-24
780776	'TVP23A'	mRNA	2.584963	2.2E-08	2.384664	1.51E-06	2.979822	2.54E-12
8578	'SCARF1'	mRNA	2.5542	2.44E-17	1.740613	2.11E-06	2.139163	7.79E-11
5997	'RGS2'	mRNA	2.551796	9.54E-19	1.321928	0.000874	1.562936	1.41E-05
3164	'NR4A1'	mRNA	2.534963	7.6E-112	2.005125	2.02E-55	2.005256	1.06E-57
942	'CD86'	mRNA	2.532495	6.1E-12	2.440573	2.17E-10	2.567685	2.56E-12
5054	'SERPINE1'	mRNA	2.523167	4.9E-256	1.807355	3.25E-97	2.180972	6.9E-168
55752	'SEPTIN11'	mRNA	2.496426	4.29E-33	2.008562	1.51E-17	2.459432	1.76E-31
2048	'EPHB2'	mRNA	2.488286	1.02E-69	1.934412	2.39E-33	2.807355	1.61E-98
6710	'SPTB'	mRNA	2.478047	4.24E-27	1.813231	2.23E-11	2.378512	5.33E-24
1E+08	'GOLGA8F'	mRNA	2.428179	1.39E-13	2.075081	1.19E-08	1.679906	1.64E-05
51733	'UPB1'	mRNA	2.415037	3.9E-09	1.906891	5.95E-05	1.874469	0.000058
2065	'ERBB3'	mRNA	2.387023	1.54E-09	2.321928	1.62E-08	2.603341	6.28E-12
3303	'HSPA1A'	mRNA	2.383699	0	1.038212	2.33E-52	1.14591	1.15E-70
7292	'TNFSF4'	mRNA	2.340289	7.9E-132	2.033369	2.07E-85	2.5107	1.7E-159
2697	'GJA1'	mRNA	2.321928	0.000037	2.237039	0.000156	2.237039	0.000107
6504	'SLAMF1'	mRNA	2.321928	8.9E-06	2.169925	0.0001	2.584963	1.71E-07
3274	'HRH2'	mRNA	2.288245	2.38E-79	1.791413	4.2E-39	1.937634	5.32E-50
11318	'GPR182'	mRNA	2.25634	3.88E-11	1.959358	1.73E-07	2.530515	5.16E-15
55604	'CARMIL1'	mRNA	2.230298	4.95E-08	2.08092	1.74E-06	1.884523	2.27E-05
10148	'EBI3'	mRNA	2.215013	8.73E-24	1.61891	3.18E-10	2.30117	3.57E-26
9582	'APOBEC3E	mRNA	2.165882	1.24E-14	1.420437	4.06E-05	1.855399	9.75E-10
6375	'XCL1'	mRNA	2.123555	9.1E-136	1.928491	1E-99	1.830205	4.48E-90
3672	'ITGA1'	mRNA	2.056754	2.71E-16	1.177763	0.000245	2.053488	3.7E-16
2308	'FOXO1'	mRNA	2.021062	1.6E-22	1.393664	1.33E-08	1.985786	2.48E-21
7124	'TNF'	mRNA	2	1.68E-21	1.443607	3.66E-09	1.941106	9.94E-20
5581	'PRKCE'	mRNA	1.991176	1.44E-17	1.150243	9.94E-05	1.84212	2.66E-14
84969	'TOX2'	mRNA	1.983698	5.85E-37	1.419084	4.77E-15	1.738586	5.21E-26
59	'ACTA2'	mRNA	1.95906	2.4E-110	2.037274	4.6E-117	2.377109	3.2E-186
51513	'ETV7'	mRNA	1.954196	3.93E-10	1.841302	2.38E-08	2.544321	4.44E-20
3399	'ID3'	mRNA	1.937587	3.57E-48	1.3901	1.21E-19	1.335823	8.19E-19
3434	'IFIT1'	mRNA	1.928917	1.45E-10	2.013806	3.21E-11	2.321928	7.08E-17
7052	'TGM2'	mRNA	1.928917	1.45E-10	1.365649	0.000131	2.428843	4.54E-19
3543	'IGLL1'	mRNA	1.911191	2.2E-25	1.928264	9.21E-25	2.16273	6.5E-35
728113	'ANXA8L1'	mRNA	1.887127	3.01E-07	2.024128	4.66E-08	2.178442	5.07E-10
1495	'CTNNA1'	mRNA	1.87192	8.49E-73	1.33309	5.09E-29	1.655574	2.27E-52
115019	'SLC26A9'	mRNA	1.861227	2.82E-69	1.630162	1.4E-46	1.979924	8.83E-81
3433	'IFIT2'	mRNA	1.85536	1.37E-26	1.500265	8.05E-15	2.435067	5.75E-55
72	'ACTG2'	mRNA	1.851749	2.18E-22	1.851749	2.64E-21	2.280771	1.31E-38
4689	'NCF4'	mRNA	1.836501	0.000019	1.747234	0.00012	2.099536	2.37E-07
57224	'NHSL1'	mRNA	1.82362	3.26E-21	1.36257	6.65E-10	2.083416	1.01E-29

3662	'IRF4'	mRNA	1.807355	3.72E-19	1.481869	3.65E-11	1.876729	7.13E-21
3693	'ITGB5'	mRNA	1.796467	9.75E-07	1.881356	3.93E-07	1.961526	3.35E-08
23462	'HEY1'	mRNA	1.795642	2.76E-17	1.294447	1.52E-07	1.647119	7.56E-14
6539	'SLC6A12'	mRNA	1.794083	1.98E-49	1.630477	1.19E-36	1.748021	9.92E-46
64359	'NXN'	mRNA	1.77259	0.000191	2.169925	1.09E-06	2.345775	2.03E-08
1846	'DUSP4'	mRNA	1.748414	2.2E-107	1.046794	3.07E-28	1.603341	7.17E-85
24	'ABCA4'	mRNA	1.742504	9.24E-16	1.321928	9E-08	1.950612	9.51E-21
2334	'AFF2'	mRNA	1.736966	3.3E-16	1.404984	3.13E-09	2	5.8E-23
4052	'LTBP1'	mRNA	1.722466	5.75E-12	1.087463	0.000373	1.378512	4.01E-07
81855	'SFXN3'	mRNA	1.703282	2.22E-11	1.668794	2.87E-10	1.597241	1.09E-09
718	'C3'	mRNA	1.693022	7.95E-09	1.616671	1.64E-07	1.925999	6.41E-12
80119	'PIF1'	mRNA	1.651052	8.04E-17	1.219169	8.11E-08	1.442943	4.48E-12
140685	'ZBTB46'	mRNA	1.647328	1.84E-21	1.3254	5.53E-12	1.464164	5.91E-16
3398	'ID2'	mRNA	1.6386	2.08E-22	1.268489	1.99E-11	1.816693	8.95E-29
169611	'OLFML2A'	mRNA	1.630766	2.44E-08	1.31259	6.55E-05	1.67516	8.71E-09
7421	'VDR'	mRNA	1.622195	5.26E-13	1.316259	1.45E-07	1.487446	1.67E-10
9595	'CYTIP'	mRNA	1.61891	8.34E-11	1.251539	9.87E-06	1.280108	2.38E-06
1026	'CDKN1A'	mRNA	1.596644	3.11E-10	1.314873	3.1E-06	1.664816	3.51E-11
57535	'ELAPOR1'	mRNA	1.594153	3.51E-94	1.540684	1.46E-81	1.532785	2.41E-84
8736	'MYOM1'	mRNA	1.584963	3.92E-05	1.452512	0.000465	1.533432	9.62E-05
121549	'ASCL4'	mRNA	1.581171	5.18E-58	1.01694	1.26E-18	1.60003	4.55E-59
91543	'RSAD2'	mRNA	1.568752	3.04E-40	1.116097	1.48E-16	1.803897	7.49E-57
8638	'OASL'	mRNA	1.567685	4.34E-13	1.392317	2.41E-09	2.050626	2.09E-25
653145	'ANXA8'	mRNA	1.566227	2.55E-08	1.783038	8.35E-11	1.95425	3.83E-14
94240	'EPSTI1'	mRNA	1.556592	7.89E-64	1.292883	8.52E-38	1.696239	1.7E-78
495	'ATP4A'	mRNA	1.545968	2.13E-11	1.807355	8.45E-16	1.298658	1.29E-07
22822	'PHLDA1'	mRNA	1.536053	0.000051	1.432959	0.00041	1.510962	8.45E-05
171177	'RHOV'	mRNA	1.488286	9.2E-08	1.584963	1.9E-08	1.906891	8.57E-14
54478	'PIMREG'	mRNA	1.479743	1.76E-21	1.503279	5.01E-21	1.401741	1.22E-18
94015	'TTYH2'	mRNA	1.459432	0.000854	1.554589	0.000464	1.643856	9.29E-05
9047	'SH2D2A'	mRNA	1.444529	2.41E-21	1.378512	6.52E-18	1.187933	2.3E-13
6764	'DENND2B'	mRNA	1.439112	5.04E-10	1.13245	0.000014	1.489385	1E-10
1475	'CSTA'	mRNA	1.436099	9.49E-25	1.265684	3.94E-17	1.810383	9.86E-44
2027	'ENO3'	mRNA	1.411814	2.86E-10	1.099536	1.37E-05	1.215013	2.66E-07
3437	'IFIT3'	mRNA	1.407806	6.02E-26	1.054918	3.1E-12	1.692933	2.39E-40
9734	'HDAC9'	mRNA	1.404728	2.71E-80	1.037553	7.84E-36	1.223696	1.54E-56
5652	'PRSS8'	mRNA	1.383329	0.000149	2.705257	3.05E-22	2.476438	7E-18
50937	'CDON'	mRNA	1.369573	3E-22	1.219381	8.44E-16	1.563746	2.37E-30
286676	'ILDR1'	mRNA	1.321928	0.000135	1.469485	2.27E-05	1.387023	5.32E-05
10112	'KIF20A'	mRNA	1.30212	3.1E-74	1.456448	6.63E-92	1.238694	8.84E-65
27074	'LAMP3'	mRNA	1.297053	4.3E-130	1.017617	5.46E-67	1.249873	5.3E-117
1491	'CTH'	mRNA	1.296217	5.72E-49	1.152003	2.74E-34	1.364852	9.6E-55
3587	'IL10RA'	mRNA	1.284789	4.87E-25	1.096344	4.71E-16	1.516962	5.59E-37
9232	'PTTG1'	mRNA	1.279503	8.12E-57	1.502702	1.88E-79	1.372436	1.97E-66
3604	'TNFRSF9'	mRNA	1.278742	2.51E-50	1.069837	1.84E-30	1.387706	1.49E-60
3112	'HLA-DOB'	mRNA	1.270854	7.61E-07	1.015597	0.00045	1.487665	1.46E-09
3119	'HLA-DQB1	mRNA	1.270591	4.1E-176	1.05885	8.4E-105	1.244334	9.3E-165

199223	'TTC21A'	mRNA	1.263034	5.4E-06	1.307429	4.95E-06	1.137504	8.39E-05
5972	'REN'	mRNA	1.261807	6.32E-26	1.130124	1.37E-18	1.258734	2.03E-25
3627	'CXCL10'	mRNA	1.254997	2.6E-10	1.246915	1.75E-09	1.771181	4.34E-23
6752	'SSTR2'	mRNA	1.249108	2.76E-05	1.429988	1.09E-06	1.584963	7.52E-09
2669	'GEM'	mRNA	1.242857	2.98E-08	1.011973	5.21E-05	1.104337	2.34E-06
388960	'C2orf78'	mRNA	1.222392	8.69E-05	1.555519	1.74E-07	1.479168	5.14E-07
9564	'BCAR1'	mRNA	1.211504	1.16E-09	1.018859	3.42E-06	1.186701	4.14E-09
5552	'SRGN'	mRNA	1.203812	3.7E-150	1.258385	1.1E-155	1.213933	1.1E-150
57699	'CPNE5'	mRNA	1.182203	0.000998	1.509014	0.000011	1.584963	1.24E-06
3597	'IL13RA1'	mRNA	1.180572	0.000376	1.415037	1.37E-05	1.242857	0.000161
84722	'PSRC1'	mRNA	1.164631	4.94E-20	1.062061	5.38E-15	1.092118	4.86E-17
3115	'HLA-DPB1'	mRNA	1.161244	6.8E-140	1.049074	4.2E-101	1.121961	1.3E-126
9580	'SOX13'	mRNA	1.137504	7.19E-05	1.392317	6.44E-07	1.364572	5.74E-07
2260	'FGFR1'	mRNA	1.089267	4.13E-05	1.252766	2.53E-06	1.145851	1.44E-05
83461	'CDCA3'	mRNA	1.088853	9.02E-23	1.203689	1.06E-26	1.060785	4.11E-21
7136	'TNNI2'	mRNA	1.05153	1.95E-05	1.447459	4.65E-10	1.306103	2.14E-08
8022	'LHX3'	mRNA	-1	1.13E-06	-1.09192	4.57E-08	-1.05445	2.49E-07
1.01E+08	'PMF1-BGL	mRNA	-1.0206	1.27E-05	-1.32838	2.71E-08	-2.18773	1.91E-15
10235	'RASGRP2'	mRNA	-1.0217	7.49E-06	-1.13535	3.4E-07	-1.13535	6.87E-07
283417	'DPY19L2'	mRNA	-1.02385	1.11E-07	-1.03997	2.09E-08	-1.26777	1.24E-10
54498	'SMOX'	mRNA	-1.07916	2.54E-74	-1.00161	1.73E-71	-1.23853	3.48E-94
65998	'ZFTA'	mRNA	-1.08873	1.4E-12	-1.09954	1.08E-13	-1.61566	9.26E-23
146713	'RBFOX3'	mRNA	-1.08927	5.22E-05	-1.47393	7.93E-08	-2.25154	8.92E-13
4068	'SH2D1A'	mRNA	-1.08998	9.93E-10	-1.08998	2.11E-10	-1.35588	1.37E-13
83637	'ZMIZ2'	mRNA	-1.10429	5.2E-121	-1.07602	1.9E-125	-1.19141	5.1E-139
116151	'FAM210B'	mRNA	-1.12114	1.02E-13	-1.03926	3.78E-13	-1.11064	8.99E-14
653082	'ZDHHC11E	mRNA	-1.19745	2.78E-06	-1.80465	1.29E-11	-1.47632	1.62E-08
203427	'SLC25A43'	mRNA	-1.20716	1.71E-08	-1.29462	6.43E-10	-1.20716	1.24E-08
399668	'SMIM10L2	mRNA	-1.21791	3.8E-06	-1.1565	4.6E-06	-1.57154	9.64E-09
3762	'KCNJ5'	mRNA	-1.2363	6.98E-08	-1.64256	2.48E-12	-1.54757	4.95E-11
79850	'TLCD3A'	mRNA	-1.24031	4.85E-20	-1.1193	2.23E-18	-1.08651	1.14E-16
9619	'ABCG1'	mRNA	-1.24457	4.96E-31	-1.58986	3.23E-47	-1.81225	2.04E-54
84216	'TMEM117	mRNA	-1.25054	0.000199	-1.40808	2.33E-05	-1.20163	0.000285
9423	'NTN1'	mRNA	-1.27854	7.76E-08	-1.27854	2.85E-08	-1.94596	7.71E-14
84662	'GLIS2'	mRNA	-1.31797	5.25E-11	-1.15024	1.23E-09	-1.29834	6.09E-11
404281	'YY2'	mRNA	-1.32193	4.42E-05	-1.37084	1.45E-05	-1.27462	6.47E-05
114879	'OSBPL5'	mRNA	-1.32805	1.59E-07	-1.21022	5.21E-07	-1.15472	2.55E-06
29958	'DMGDH'	mRNA	-1.32938	2.5E-28	-1.38268	6.37E-32	-1.71239	1.77E-41
9118	'INA'	mRNA	-1.33121	1.53E-18	-1.24101	8.48E-18	-1.31962	1.37E-18
339983	'NAT8L'	mRNA	-1.33985	1.65E-05	-1.09192	0.000179	-1.05445	0.000405
80201	'HKDC1'	mRNA	-1.34593	1.4E-23	-1.08289	3.3E-18	-1.56677	7.38E-30
85462	'FHDC1'	mRNA	-1.37022	3E-15	-1.10463	7.08E-12	-1.16993	2.66E-12
10765	'KDM5B'	mRNA	-1.38143	8.45E-07	-1.30743	1.19E-06	-1.58496	3.05E-08
4239	'MFAP4'	mRNA	-1.39689	1.73E-10	-1.60334	2.67E-13	-1.81193	4.32E-15
1047	'CLGN'	mRNA	-1.3995	5.51E-52	-1.64886	9.36E-70	-1.71571	7.43E-71
92691	'TMEM169	mRNA	-1.40054	5.64E-13	-1.10579	7.58E-10	-1.36257	1.14E-12
113730	'KLHDC7B'	mRNA	-1.40074	1.98E-52	-1.44699	2.17E-58	-1.2293	1.25E-43

11247	'NXPH4'	mRNA	-1.44663	1.25E-31	-1.14965	6.1E-24	-1.72792	2.56E-41
283229	'CRACR2B'	mRNA	-1.45943	2.62E-07	-1.1375	1.47E-05	-1.34395	1.19E-06
7325	'UBE2E2'	mRNA	-1.48302	0.000354	-1.52937	0.000129	-1.84594	1.97E-05
5457	'POU4F1'	mRNA	-1.5025	2.05E-12	-1.62803	1.53E-14	-1.52675	7.11E-13
727	'C5'	mRNA	-1.5115	4.75E-10	-1	4.65E-06	-1.28473	3.61E-08
146439	'BICDL2'	mRNA	-1.5502	0.000866	-1.65711	0.000325	-1.89812	9.01E-05
27443	'CECR2'	mRNA	-1.56478	5.48E-06	-1.50589	5.89E-06	-1.14975	0.000388
54514	'DDX4'	mRNA	-1.58496	1.54E-16	-1.34239	7.61E-14	-1.56478	1.82E-16
138151	'NACC2'	mRNA	-1.58496	8.46E-09	-1.58496	3.31E-09	-2.75489	4.3E-17
4636	'MYL5'	mRNA	-1.61073	2.31E-09	-1.42786	2.21E-08	-1.14775	4.85E-06
26872	'STEAP1'	mRNA	-1.61667	8.03E-08	-2.27563	3E-12	-1.87971	1.49E-09
114804	'RNF157'	mRNA	-1.61669	2.04E-10	-1.42466	3.29E-09	-2.40224	4.92E-17
2516	'NR5A1'	mRNA	-1.66588	6.74E-14	-1.43558	5.96E-12	-1.1765	1.05E-08
2593	'GAMT'	mRNA	-1.67807	1.62E-08	-1	0.000136	-1.54057	9.95E-08
1291	'COL6A1'	mRNA	-1.70036	0	-1.19741	6.1E-225	-1.90035	0
51226	'COPZ2'	mRNA	-1.72583	5.38E-08	-1.17834	3.62E-05	-1.9027	4.1E-09
84460	'ZMAT1'	mRNA	-1.74543	1.15E-05	-1.926	1.45E-06	-1.66297	2.06E-05
11076	'TPPP'	mRNA	-1.76553	3.15E-05	-1.28011	0.000938	-1.58496	0.000115
26038	'CHD5'	mRNA	-1.77761	3.09E-11	-1.38333	1.72E-08	-1.48063	5.79E-09
643965	'TMEM88B'	mRNA	-1.80735	1.67E-14	-1.01886	5.17E-07	-1.38414	2.88E-10
1.08E+08	'LOC10798'	mRNA	-1.80735	0.000143	-2.22239	7.35E-06	-1.58496	0.000537
374654	'KIF7'	mRNA	-1.848	2.03E-07	-1.46949	7.53E-06	-1.52607	5.98E-06
4897	'NRCAM'	mRNA	-1.92184	6.07E-48	-2.01495	2.54E-53	-2.51245	1.67E-67
1292	'COL6A2'	mRNA	-2.04454	0	-1.41284	1.4E-249	-2.31689	0
4118	'MAL'	mRNA	-2.07455	1.28E-30	-1.32453	1.69E-17	-2.07455	6.07E-31
152273	'FGD5'	mRNA	-2.25873	9.21E-09	-1.11189	0.000617	-1.74416	1.41E-06
26086	'GPSM1'	mRNA	-2.4134	9.21E-39	-1.5509	5.85E-23	-2.17239	1.66E-34
387357	'THEMIS'	mRNA	-2.44478	3.45E-07	-4.61471	3.76E-12	-3.61471	2.93E-10
26108	'PYGO1'	mRNA	-2.62449	5.17E-06	-1.88753	0.000187	-2.20945	3.92E-05
54549	'SDK2'	mRNA	-2.6477	3.06E-14	-1.74723	3.65E-09	-2.85415	1.66E-15
267004	'PGBD3'	mRNA	-2.71097	0.000085	-11.4252	3.95E-08	-2.92537	2.06E-05
164832	'LONRF2'	mRNA	-2.79008	2.38E-13	-1.42084	2.42E-06	-2.12711	4.6E-10
9805	'SCRN1'	mRNA	-2.80735	3.16E-08	-1.36678	0.000639	-2.44478	2.96E-07
50614	'GALNT9'	mRNA	-3.24793	2.07E-07	-2.66297	2.14E-06	-4.24793	5.41E-09
3768	'KCNJ12'	mRNA	-3.45943	7.58E-07	-3.45943	5.4E-07	-3.04439	3.01E-06
3485	'IGFBP2'	mRNA	-3.6017	4.4E-120	-2.6757	4.97E-93	-3.81929	9.7E-127
445329	'SULT1A4'	mRNA	-9.78753	4.16E-57	-9.99904	2.68E-58	-1.32624	4.71E-12
1.1E+08	'LOC11038'	mRNA	-10.7879	3.53E-05	-10.7879	3.04E-05	-10.7879	3.31E-05
8363	'H4C11'	mRNA	-11.0362	2.66E-06	-11.0362	2.16E-06	-11.0362	2.43E-06

Accession	Description	Coverage [	# Peptides	# PSMs	# Unique P	# AAs	MW [kDa]	calc. pI	Score Mas
H6VRG1	Keratin, typ	23	15	75	13	645	66.1	8.12	1173
Q53HL1	Myosin reg	51	8	74	1	171	19.8	4.84	1422
J3QRS3	Myosin ligh	50	8	73	1	177	20.4	4.75	1390
G3V1V0	Myosin ligh	52	9	31	9	161	18	4.77	589
P35527	Keratin, typ	22	10	37	10	623	62	5.24	683
A0A1B0GV	Keratin 10	13	9	37	8	624	63.3	5.26	634
A0A0S2Z42	HCG20398	17	9	22	7	564	60	8	286
P35908	Keratin, typ	14	8	21	7	639	65.4	8	283
P62269	Small ribos	32	5	23	5	152	17.7	10.99	320
P05387	Large ribos	53	4	9	4	115	11.7	4.54	174
Q59FI9	60S riboso	24	3	12	3	197	21.5	10.1	317
P60709	Actin, cyto	19	6	16	5	375	41.7	5.48	208
P08779	Keratin, typ	9	4	14	2	473	51.2	5.05	236
A1A508	PRSS3 prot	9	2	31	1	247	26.5	7.21	398
P13647	Keratin, typ	8	5	14	3	590	62.3	7.74	112
P62263	Small ribos	16	2	12	2	151	16.3	10.05	280
P62913	Large ribos	20	3	8	3	178	20.2	9.6	262
V9HWI5	Cofilin 1 (N	29	4	10	4	166	18.5	8.09	180
S6AWD6	IgG L chain	9	1	8	1	178	19.4	8.46	212
P02533	Keratin, typ	7	3	10	1	472	51.5	5.16	129
B4DR52	Histone H2	21	3	6	3	166	18	10.32	104
A8MUS3	Ribosomal	12	2	9	2	194	21.9	10.48	158
P62280	Small ribos	24	4	6	4	158	18.4	10.3	95
E7EQ64	Serine prot	11	2	31	1	261	28.1	7.25	306
F8WCF6	Actin-relat	21	4	9	4	181	21	8.76	80
P46776	Large ribos	22	3	9	3	148	16.6	11	169
B2RB90	glutamine-	2	1	2	1	682	76.9	7.25	108
Q8WVX7	40S riboso	24	4	11	4	157	17.3	10.52	129
P62277	Small ribos	21	3	7	3	151	17.2	10.54	116
Q562M3	Actin-like p	28	2	5	1	103	11.5	6.68	53
B2R4C0	60S riboso	15	2	4	2	176	20.7	10.71	89
P62851	Small ribos	22	3	7	3	125	13.7	10.11	106
A1LUY1	60S riboso	15	2	7	2	117	13.3	11.47	120
B4DPP6	cDNA FLJ54	4	2	3	2	618	70.3	6.09	76
A1A4E9	Keratin 13	4	2	7	1	458	49.6	4.96	133
P35268	Large ribos	19	2	5	2	128	14.8	9.19	70
A0A024R9I	60S riboso	24	2	3	2	115	12.8	9.63	80
H0YKD8	60S riboso	13	2	7	2	170	19.1	11.46	85
B2R4D8	60S riboso	28	3	7	3	136	15.8	10.56	74
A0A5C2GG	IGH + IGL c	10	1	4	1	109	11.8	8.88	79
A0A5C2FT\	IGL c14_lig	10	1	5	1	108	11.8	8.46	94
B2R4R0	Histone H4	17	2	4	2	103	11.4	11.36	59
A0A5C2GN	IG c742_lig	11	1	1	1	103	11.4	8	63
B2R4P2	cDNA, FLJ9	11	2	8	2	199	22.2	8.38	83
P61254	Large ribos	15	2	4	2	145	17.2	10.55	50
B7Z268	Single-stra	9	1	2	1	159	18.5	10.1	52

A0A0A6YYI	60S ribosoı	4	1	4	1	228	26.4	10.1	89
A0A5C2GT(	IG c541_lig	7	1	4	1	111	12.1	5.01	66
B7Z4C8	60S ribosoı	11	1	2	1	130	15.1	10.37	54
P62829	Large ribos	16	2	3	2	140	14.9	10.51	44
A8K517	40S ribosoı	8	1	3	1	143	15.8	10.49	51
P62249	Small ribos	13	2	3	2	146	16.4	10.21	29
P62081	Small ribos	5	1	4	1	194	22.1	10.1	73
A8K486	Peptidyl-pr	5	1	4	1	165	18	6.9	82
A0A2R8Y5\	60S ribosoı	5	1	4	1	220	25	9.74	66
P60981	Destrin OS=	7	1	1	1	165	18.5	7.85	48
A0A024R2:	Interferon	14	1	1	1	125	13.9	7.93	46
B2R4D5	Actin-relat(	6	1	2	1	178	20.5	8.59	
A0A5C2FV\	IGL c794_li	7	1	1	1	111	11.6	5.81	48
E9N3C0	Non-struct	1	1	2	1	1765	193.5	7.58	
A0A7P0S5H	40S ribosoı	8	1	2	1	136	15.3	9.35	46
P81605	Dermcidin	10	1	4	1	110	11.3	6.54	75
B0I1T2	Unconvent	1	1	2	1	1018	116.4	8.73	44
A0A024R4I	40S ribosoı	5	1	1	1	194	22.6	10.65	37
A0A5C2GI7	IG c217_lig	6	1	4	1	110	11.7	8.47	39
A0A5C2FT\	IGL c142_li	10	1	2	1	108	11.6	7.99	33
A0A0S2UT:	Pol protein	4	1	1	1	306	34.8	9.14	0
Q6ZRX7	cDNA FLJ46	17	1	3	1	157	16.7	8.07	
Q59EA2	Coronin (Fr	2	1	2	1	501	56.3	8.19	40
K7ELC2	40S ribosoı	8	1	1	1	152	17.7	10.39	
A0A8I5KW7	Myosin hea	1	1	2	1	1981	229	5.64	30
A0A8J2HSV	Similar to M	1	1	4	1	896	103.6	5.83	
A0A024RB:	40S ribosoı	8	1	1	1	115	13	11	
Q8TF72	Protein Shr	0	1	1	1	1996	216.7	7.8	27
L8E7Q1	Alternative	20	1	1	1	46	5.3	10.84	
A0A5C2G3	IGL c3752_	7	1	1	1	113	12.5	7.12	
A0A5C2G8(	IGL c320_li	10	1	1	1	107	11.7	8.85	
A0A3S7TE(	Pol protein	1	1	2	1	1003	113.4	8.12	0

Score Sequ	# Peptides	# Peptides (by Search Engine): Sequest HT
85.23	14	15
94.65	8	8
89.58	7	8
32.93	8	6
46.66	10	10
48.18	9	8
34.18	8	8
22.93	7	8
27.64	5	5
15.2	3	4
18.54	3	3
12.61	6	5
17.49	4	4
29.44	2	2
21.59	4	4
16.79	2	2
6.74	3	1
5.04	4	3
11.45	1	1
12.66	3	3
6.58	3	3
15.77	2	2
5.58	4	2
28.38	2	2
7.05	4	2
10.19	3	3
3.87	1	1
11.06	3	4
5.09	3	2
7.29	2	2
4.99	2	2
6.47	3	2
5.79	2	1
3.28	2	1
9.45	1	2
7.9	1	2
2.39	2	1
8.44	2	2
7.35	3	2
2.69	1	1
7.78	1	1
3.64	2	2
	1	
9.99	2	2
2.7	1	1
3.7	1	1

3.93	1	1
3.52	1	1
2.92	1	1
2.55	2	1
4.35	1	1
2.28	2	1
4.5	1	1
3.62	1	1
1.66	1	1
	1	
	1	
2.4		1
	1	
1.85		1
3.57	1	1
3.86	1	1
2.19	1	1
	1	
0	1	1
2.37	1	1
	1	
0		1
1.87	1	1
0		1
0	1	1
0		1
1.85		1
	1	
0		1
0		1
0		1
	1	